J. Fluid Mech. (1988), *vol.* 190, *pp.* 1–37
Printed in Great Britain

Experimental and numerical investigation of the three-dimensional transition in plane wakes

By E. MEIBURG† AND J. C. LASHERAS‡

† Division of Applied Mathematics, Brown University, Providence, RI 02912, USA
‡ Department of Mechanical Engineering, University of Southern California, Los Angeles, CA 90089-1453, USA

(Received 9 March 1987 and in revised form 25 August 1987)

The three-dimensional structure of a moderate-Reynolds-number (≈ 100) plane wake behind a flat plate subjected to periodic spanwise perturbations has been studied both experimentally and numerically. Comparisons between experimental interface visualizations and numerical calculations demonstrate that important features of the development of the three-dimensional evolution can be reproduced by numerical inviscid vortex dynamics.

It is shown that the redistribution, reorientation and stretching of vorticity leads to the formation of counter-rotating pairs of streamwise vortices which superimpose onto the spanwise Kármán-like vortices. These streamwise vortices exhibit lambda-shaped structures and are located in the braids connecting consecutive Kármán vortices of opposite sign.

The interaction of the evolving streamwise structure with the spanwise Kármán vortices results in the formation of closed vortex loops. Depending on the orientation of the initial perturbation, the three-dimensional vorticity field of the wake acquires either a symmetric or a non-symmetric configuration. Under the effect of a periodic vertical perturbation, the wake develops a non-symmetric vorticity mode exhibiting a staggered array of closed vortex loops of alternating sign. In contrast, under the effect of a periodic horizontal perturbation, the wake acquires a symmetric vorticity mode with the closed vortex loops of alternating sign aligned in the flow direction.

1. Introduction

It has long been established that wake flows behind two-dimensional bodies at moderate and high Reynolds numbers can exhibit coherent vortical structures (Roshko 1954; Morkovin 1964; Berger & Wille 1972; Taneda 1977). The formation of these vortical structures, as well as their two- and three-dimensional evolution, is of special interest since they determine not only the drag but also the unsteady forces acting on the body. From a more fundamental point of view, the study of the instability mechanisms resulting in the formation of two- and three-dimensional vortical structures can contribute to our understanding of laminar-turbulent transition and lead to ways to actively control the features of the flow.

Early correlation measurements by Grant (1958) show that the turbulent wake, after initially being dominated by two-dimensional Kármán-like vortices, develops strong three-dimensional vortical structures that occur in counter-rotating pairs inclined to the plane of the wake. Structures similar to these 'vortex pair eddies' or 'double roller eddies' were also observed and described by Payne & Lumley (1967), Townsend (1979), and Mumford (1983), among others. Roshko (1976) suggested that

the underlying mechanism responsible for the formation of these structures could be related to the formation of closed vortex loops. Closed loops were observed in the plan-view flow visualizations of three-dimensional plane wakes studied by Breidenthal (1980). In the transitional regime, Cimbala (1985) has also observed streakline patterns that seem to indicate the emergency of a three-dimensional structure. However, up to now, a complete understanding of the nature and evolution of the three-dimensional instability mechanism of the wake behind two-dimensional bodies has not yet been achieved.

Recent experimental results (Lasheras, Cho & Maxworthy 1986; Lasheras & Choi 1988) and numerical calculations (Corcos & Lin 1984; Ashurst & Meiburg 1988) indicate that the origin of the three-dimensional vortices in a plane free shear layer lies in the instability of the strain regions (braids) formed as the primary, two-dimensional, Kelvin–Helmholtz instability develops. The structure of the vorticity field in plane wakes and free shear layers differs significantly, since the wake exhibits two equally strong layers of opposite vorticity versus one dominating sign of vorticity in the shear layer. In plane wake flows, the primary instability results in the formation of strong, two-dimensional vortices of alternating signs, i.e. the two-dimensional Kármán vortex street. The existence of regions of positive strain between these two-dimensional, spanwise vortices suggests that a similar vortex-stretching mechanism, in a modified form, might also account for the three-dimensional transition in the wake.

To gain further insight into the three-dimensional structure of plane wake flows, and in particular to investigate the origin of the three-dimensional vorticity, we have undertaken a combined experimental and numerical analysis of the evolution of a laminar plane wake subjected to three-dimensional disturbances periodically distributed along the span. Specifying certain initial perturbations to the purely two-dimensional flow and subsequently tracking them well into the nonlinear regime offers a means of studying the instability mechanisms which lead to the three-dimensional transition in this type of flow.

We studied the flow numerically by means of three-dimensional inviscid vortex dynamics. This technique has already proven reliable for modelling two-dimensional wakes. Aref & Siggia (1981) and Meiburg (1987) have shown that important features of the initial evolution of the two-dimensional wake can be reproduced by numerical simulations based on the assumption of nearly inviscid vortex dynamics. Ashurst & Meiburg (1988) have recently studied three-dimensional plane free shear layers by means of the vortex-filament technique. Comparisons between their calculations and the flow visualizations of Lasheras & Choi (1988) demonstrated that the three-dimensional evolution of a plane shear layer created behind a flat plate by two laminar streams can be modelled via inviscid vortex dynamics. Although the presence of two equally strong layers of opposite vorticity in the wake leads to a much more complicated structure of the vorticity field, it was anticipated that the initial stages of development of a three-dimensional plane wake could also be analysed on the basis of its vorticity dynamics. This numerical approach is, of course, limited since viscous effects such as those leading to the break-up and re-linking of vortex tubes, viscous diffusion of vorticity or cancellation of vorticity of opposite signs are not accounted for. However, in the case of the wake formed behind a flat plate separating two laminar streams with laminar boundary layers, the numerical method can simulate the evolution of the smooth vorticity into vortex tubes, thus providing an important insight into the nature of the underlying physical processes

dominating the initial stages of the flow, i.e. the redistribution and stretching of vorticity.

In a recent note (Meiburg & Lasheras 1987), we presented some preliminary experimental and numerical results which indicated that vortex dynamics methods could be used to model the three-dimensional transition in plane wake flows. In this paper we are extending the preliminary study and are now aiming at investigating the mechanisms responsible for the three-dimensional transition. We will analyse these mechanisms through a comparative study between numerical vortex dynamics simulations and flow visualizations of plane wakes subjected to periodic spanwise perturbations.

The organization of this paper is as follows: we will discuss the experimental techniques and flow-visualization methods in §2. In §3, the three-dimensional vortex dynamics method used for the numerical flow simulation will be described. In §4, we will first present a comparative study of the experimental and numerical results of a representative case. The suitability of inviscid vortex dynamics methods for modelling the three-dimensional transition will then be discussed. Following this analysis, a physical mechanism for the three-dimensional transition will be presented in §5. In §6, the topology of the three-dimensional vorticity field of the plane wake will be studied as a function of the initial conditions. Finally, some concluding remarks will be given in §7.

2. Experimental technique

The base-flow configuration selected for the study was the two-dimensional wake created behind a flat plate separating two laminar flows of equal velocities. The development of a three-dimensional flow structure in the plane wake was then experimentally investigated by analysing the response of the two-dimensional base flow to periodic spanwise perturbations of varying magnitude, orientation, and wavelength. The test-rig (figure 1) consisted of a water channel in which two horizontal, laminar water streams of equal velocity were produced, initially separated by a flat plate. In the test section, a plane wake was formed as the two parallel streams met at the trailing edge of the splitter plate. (A detailed description of the experimental facility can be found in Lasheras *et al.* 1986).

The base-flow condition selected for this study and used in all the experiments reported here was a horizontal plane wake formed by two water streams with equal velocities $U = 3.4$ cm/s. At the trailing edge of the splitter plate, each laminar boundary layer was 9.0 mm thick and had a momentum thickness of 1.2 mm. The Reynolds number based on the free-stream velocity and the total momentum thickness was 74.

Since any perturbation in the initial conditions can be decomposed into its spectral components, we first chose to analyse the response of the base flow to two types of sinusoidal initial perturbations. The first type consisted of introducing weak vertical vorticity of alternating signs periodically along the span. Experimentally, this was achieved by using a modified splitter plate containing a sinusoidal corrugation (figure 2). At its trailing edge, the plate had a vertical undulation of amplitude a and wavelength λ. The corrugation along the plate was gradually achieved over a length approximately 100 times the final value of its amplitude. The second type of perturbation periodically introduced along the span consisted of introducing weak vorticity in the flow direction of alternating signs. This was done experimentally by

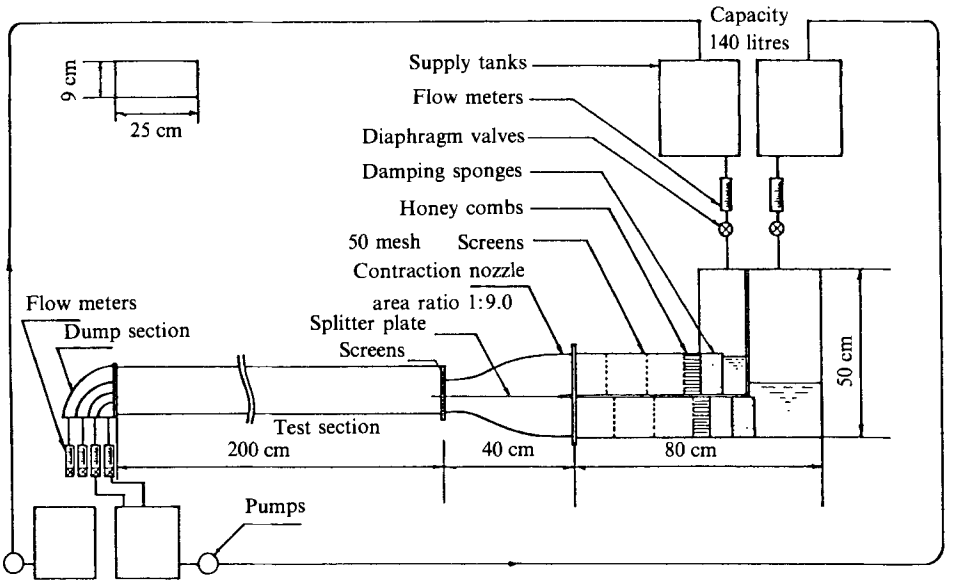

FIGURE 1. Experimental apparatus.

modifying the trailing edge of a flat splitter plate to give it a sinusoidal indentation of amplitude a wavelength λ, (figure 3).

By combining these two types of perturbations, i.e. by corrugating the indented splitter plate, we also studied the effect of simultaneous vertical (Y) and horizontal (X) disturbances. For this third type of perturbation, we limited our study to the cases where the horizontal (indentations) and vertical (corrugations) perturbations had the same wavelength.

To track the evolution of the interface separating both streams, the interface was visualized by inducing the fluorescence of fluorescin particles added to the lower stream with a set of spotlights. The spotlight arrangement and the fluorescein concentration were selected so that a shadow effect could be created by the corrugated, opaque interface, thereby showing its three-dimensionality. To create a solid, opaque effect at the interface, a large concentration of fluorescein particles was needed; however, variations of the physical properties of the water stream due to the high fluorescein concentration were negligible. A description of this visualization technique can be found in Lasheras & Choi (1988). Additional information about the temporal and spatial evolution of the interface was also obtained using laser induced fluorescence (LIF) cross-cuts of the wake along planes either perpendicular or parallel to the flow direction.

3. Numerical method

Incompressible flowfields in which the vorticity is confined to small regions can often be conveniently simulated by vortex methods (for reviews, see Leonard 1980, 1985). These numerical techniques make use of the fact that for incompressible flows, knowledge of the vorticity field suffices for the reconstruction of the velocity field via the Biot-Savart law (Batchelor 1967).

$$\boldsymbol{u}_{\mathrm{rot}}(\boldsymbol{x}) = -\frac{1}{4\pi}\int \frac{(\boldsymbol{x}-\boldsymbol{x}')\times\boldsymbol{\omega}(\boldsymbol{x}')}{|\boldsymbol{x}-\boldsymbol{x}'|^3}\,\mathrm{d}V(\boldsymbol{x}').$$

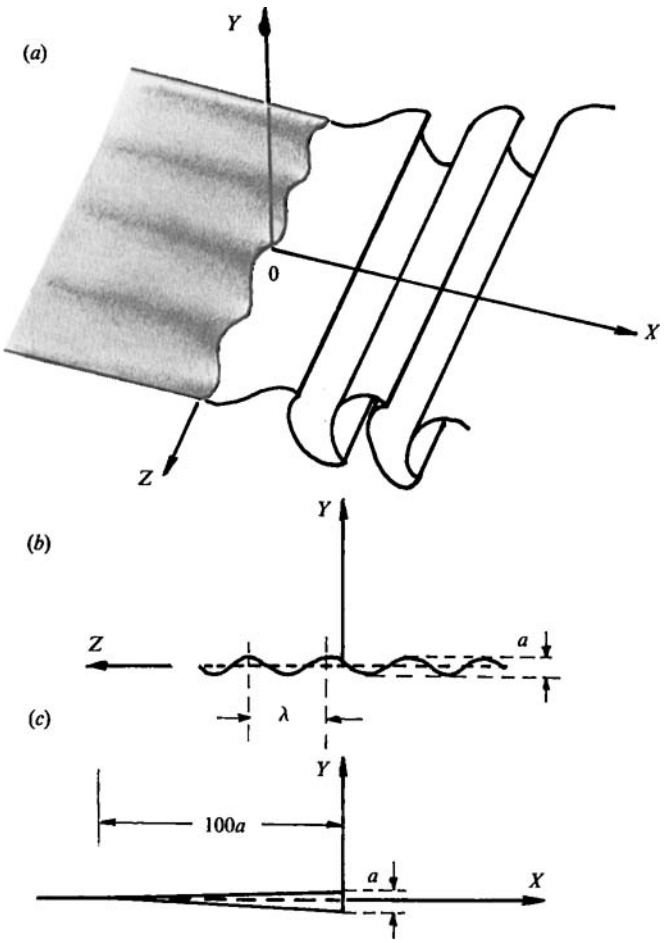

FIGURE 2. Corrugated splitter plate. (*a*) Perspective view. (*b*) End view. (*c*) Side view. The corrugation of wavelength λ and final amplitude a is gradually achieved over a length approximately $100a$.

Thus, they offer the advantage of having to discretize the rotational part of the flowfield only. Furthermore, in many cases they reduce the need to specify boundary conditions at infinity.

The specific numerical technique used in the present investigation of three-dimensional plane wakes is identical in most respects to the one used by Ashurst & Meiburg (1988) to simulate a three-dimensional, plane shear layer. Because they give a detailed description of the method, we will only give a summary of its main features here.

We limit ourselves to the analysis of the temporal problem, i.e. we consider the flowfield to be periodic both in the spanwise and in the streamwise direction, in order to be able to resolve a small section of the flow in detail. In this way, we lose the effect of streamwise variations on the evolution of the flow. This might possibly represent a serious limitation, especially in the light of findings by Koch (1985), who shows that within linear theory wake flows exhibit an absolutely unstable character. As a result, the effect of streamwise growth can influence the upstream region. The comparison with flow-visualization experiments to be presented in the following, however,

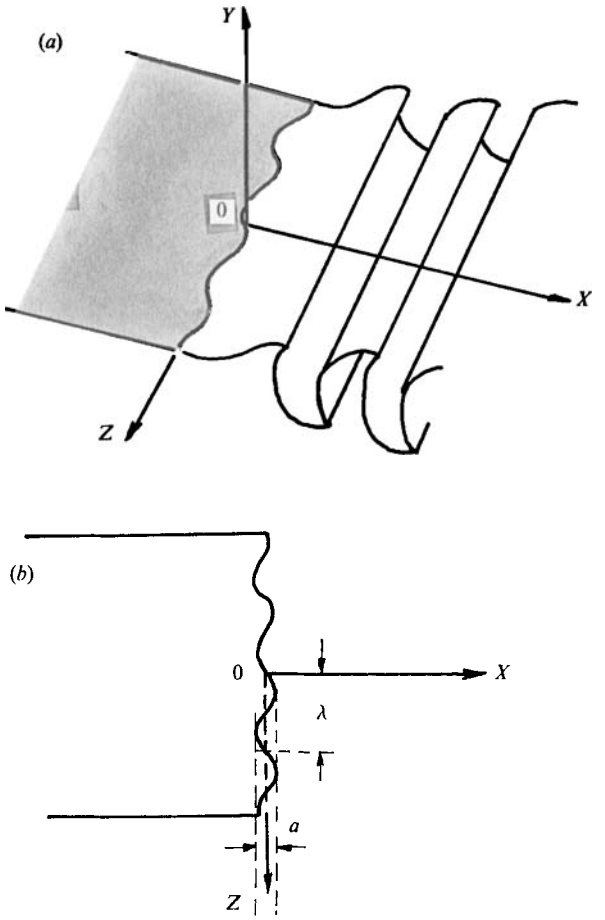

FIGURE 3. Indented splitter plate. (*a*) Perspective view. (*b*) Plan view.

indicates that the flow is simulated in a qualitatively correct manner. Thus, we believe that the nature of the mechanisms observed dominating the early stages of the three-dimensional transition would not be changed in a significant way by including streamwise variations.

We discretize the two vorticity layers representing the sides of the wake into vortex filaments with a circular cross-section over which the vorticity is distributed algebraically. The circular shape of the filament core is maintained throughout the simulation, i.e. we are neglecting its change due to the local strain field. In the course of the three-dimensional evolution, vortex stretching becomes important and the arclength of the filaments increases considerably. As a consequence, we reduce the diameter of the filaments in time so as to maintain a constant filament volume. Along the filament arclength, however, the cross-section does not vary. Our numerical model thus can correctly reproduce only scales considerably larger than the core radius.

Each filament is represented by a number of nodes along its arclength from which its shape can be reconstructed by fitting a cubic spline. As the filament arclength and curvature increases, additional nodes are introduced in order to maintain an adequate resolution. The spline representation allows us to determine the tangent vector at each nodepoint, so that the Biot–Savart integration can be carried out with

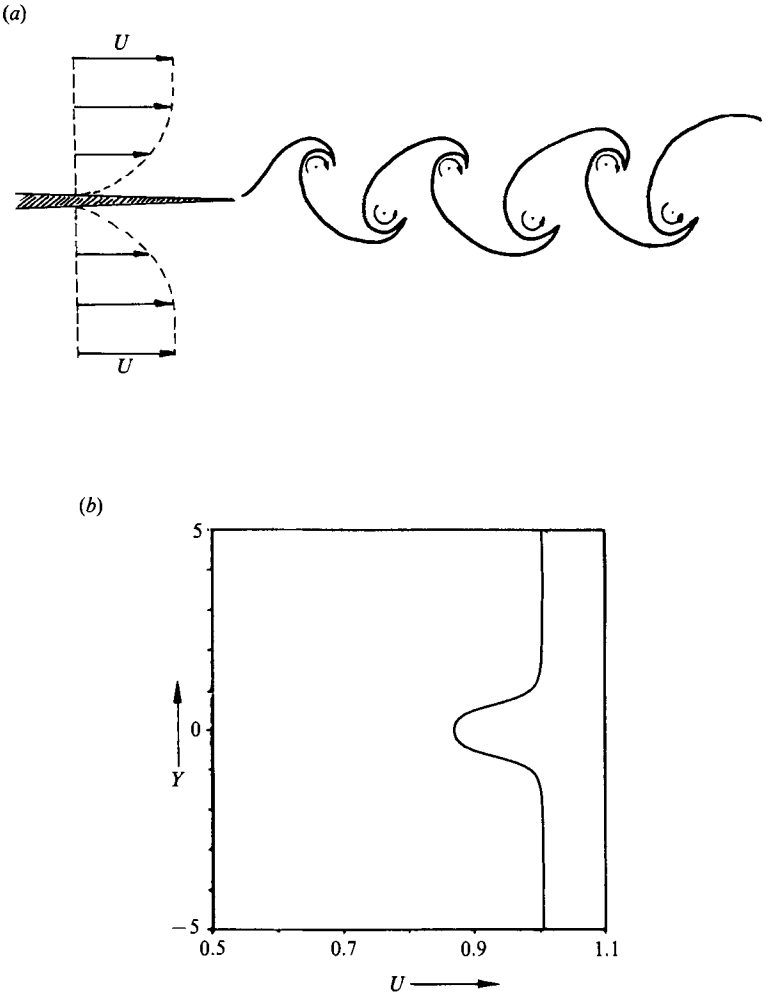

FIGURE 4. Initial velocity profile. (*a*) Experimental case; (*b*) Profile employed in the wake flow simulations.

second-order accuracy by applying the trapezoidal rule. In this way, our technique achieves higher accuracy than previously used methods employing straight line segments. All periodic images of the computational domain should contribute to the Biot–Savat integral. However, the presence of two layers of opposite vorticity causes the approximate cancellation of the effects of the remote parts of both layers. Consequently, the present code explicitly carries out the integration over the six closest images in the flow direction, while in the spanwise direction only the closest image is taken into account. Future work should aim at replacing the explicit integration by an approximation of the long-range interaction effects, thus increasing the numerical efficiency without reducing the accuracy. The flowfield is advanced in time by means of a second-order predictor–corrector timestepping scheme which allows easy introduction of additional nodes as well as the continuous reduction of the timestep as large spatial velocity gradients develop.

The diameter of the filaments at the start of the simulation represents a measure for the thickness of the rotational layer and was taken to be the unit length. The two vorticity layers are initially centred at $Y = \pm 0.65$. The free stream velocity is taken

as the reference velocity, from which then also the definition of the unit time follows as the unit length divided by the unit velocity. As a result of the initial overlap of the vorticity layers, the velocity jump of the sides of the wake, i.e. the initial wake velocity defect, is equal to 0.14, implying that we start our simulation some distance downstream of the generating body. The resulting average velocity profile is shown in figure 4(*b*).

The combination of ever increasing arclength and reduced timesteps results in exponentially increasing computational costs and presents one reason to stop the calculation at a certain time. The other reason lies in the generation of small scales, whose evolution is not accurately reproduced by the present numerical technique.

4. Response of the two-dimensional base-flow to perturbations periodically placed along the span

We first present the experimental and numerical results corresponding to a flowfield evolving from a sinusoidal, vertical spanwise perturbation with a wavelength $\frac{2}{3}$ of the most unstable streamwise wavelength of the two-dimensional base flow. To characterize the two-dimensional base flow, we initially analysed the flow beyond a flat plate with a straight trailing edge. In our experimental flow facility, the Kármán vortex street wavelength measured for the two-dimensional wake was $\lambda = 4.5$ cm. The base flow was then perturbed with a sinusoidal vertical disturbance produced by a corrugated plate (figure 2) with a sinusoidal vertical undulation of wavelength $\lambda' = 3.0$ cm ($\lambda' = \frac{2}{3}\lambda$) and amplitude $a = 3$ mm at its trailing edge.

To simulate the flow field numerically, the two sides of the wake were subjected to both a streamwise and a spanwise perturbation. The spanwise perturbation consisted of a single wave with only vertical (Y) component while the streamwise one was also a single wave with vertical (Y) component. While the streamwise perturbation will lead to the formation of the Kármán vortex street, the spanwise perturbation will cause the flow to develop a three-dimensional character. The computational domain included three wavelengths in each of these directions. The two sides of the wake initially centred at the position $Y = \pm 0.65$ were discretized into a total of 150 filaments, and each filament was represented by 27 nodepoints at the beginning. The initial disturbance consisted of a dislocation of the filament centreline in the transverse Y-direction and was identical for both sides of the wake. The wave in the streamwise X-direction had a wavelength of $\lambda = 2\pi$ and an amplitude of 0.001, whereas the one in the spanwise Z-direction had a wavelength of approximately $\lambda' = \frac{2}{3}\lambda$ and an amplitude of 0.01.

The flow visualization used in our experiments enabled us to determine the position of the three-dimensional interface separating both streams and its evolution in space and time. Although the formation of regions of concentrated vorticity can be identified by this method, our visualization did not allow for a detailed measurement of the vorticity field. Thus, for comparison purposes, the position of the interface was also calculated in the numerical simulation. To determine the position of the three-dimensional interface, uniformly distributed marker particles were inserted, initially located at the midplane between the two sides of the wake. The trajectories and positions of these particles were then calculated simultaneously with the evolution of the vorticity field. To maintain a good resolution, additional marker particles were introduced as the interface became more stretched by the development of its three-dimensionality.

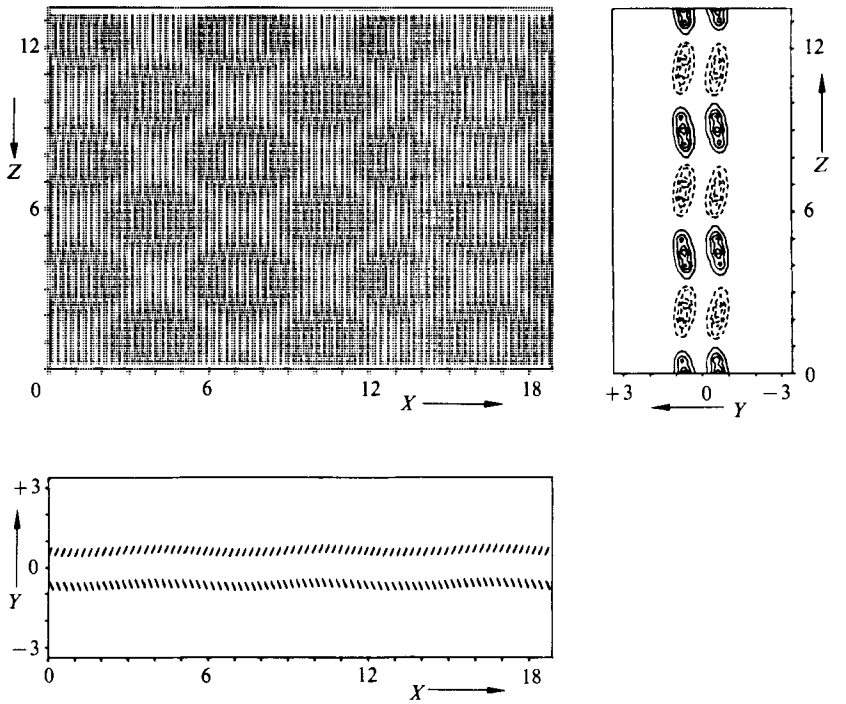

FIGURE 5. Top and side views of all vortex filaments at time $t = 90$. The filaments of the upper layer are drawn as solid lines, those of the lower layer are represented by dashed lines. In addition lines of constant streamwise vorticity are plotted for a vertical (Y, Z)-plane at $x = 4.6$.

In the following, we will first describe the computed three-dimensional evolution of the vortex filaments composing the wake. At the same time, a comparison between the experimental interface flow visualization and the numerically calculated one will be made.

Those filament sections which, as a result of the initial perturbation were displaced away from the centre of the wake into the free streams, immediately experience an acceleration in the flow direction. On the other hand, those portions displaced closer to the centre of the wake are slowed down due to the wake velocity defect. As the wavy vortex filaments tilt into the flow direction, a small streamwise component of vorticity evolves from both vorticity layers (figure 5). Simultaneously, the two-dimensional instability amplifies the initial streamwise disturbance. This instability leads to the formation of concentrated spanwise vorticity in two staggered rows, i.e. the Kármán vortex street. In the initial stages of their evolution, these spanwise rollers create a strain field, which, when viewed in a reference frame moving with the average velocity of the vorticity, has the structure qualitatively sketched in figure 6. Similar to the mixing layer, we can identify free stagnation points in the braid regions between the spanwise rollers (saddle points in the topological structure of the vector field represented by the streamlines). However, notice that even at this early stage, due to the presence of the vorticity of opposite sign, the stagnation points are not at the centre between the spanwise rollers, but slightly displaced downstream. At the stagnation points, the strain field reaches its maximum and amplifies the streamwise vorticity of those filaments left in this region of the braid. At time $t = 126.25$ in the numerical simulation, we can already identify the most stretched filaments as those residing in the region around the free stagnation points, even

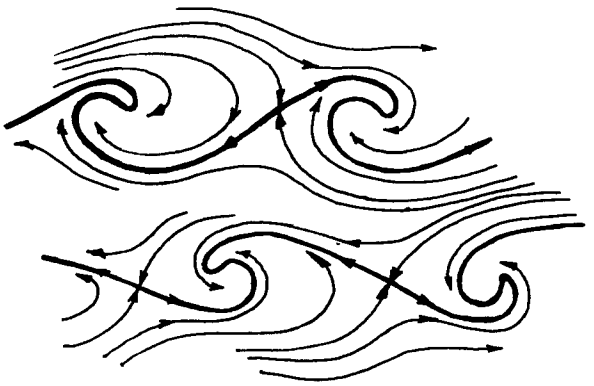

FIGURE 6. Sketch of the structure of the two-dimensional velocity field in a reference frame moving with the average velocity of the evolving Kármán vortices. Observe the presence of free stagnation points between consecutive spanwise vortices.

though the two-dimensional instability has not developed very much yet (figure 7). During this initial evolution of the vorticity, the above processes can still be viewed qualitatively as happening separately on each side of the wake. Thus, the mechanisms of concentration and stretching of vorticity are conceptually similar to the mechanisms responsible for the formation of the streamwise vorticity in plane free shear layers (Corcos & Lin 1984; Ashurst & Meiburg 1988; Lasheras & Choi 1988).

The difference between the mixing layer and the wake, however, becomes obvious as the two sides of the wake continue to interact. The reorientation of the perturbed vortex lines of the upper and lower layers from the vertical plane into the principal plane of positive strain results in the creation of streamwise vorticity of alternating signs. The evolving streamwise vorticity vectors from the two layers point in the same direction at identical streamwise and spanwise locations (figure 5). As the streamwise vortices become stronger, their vorticity concentrates and they induce in each other velocities leading to a displacement in the spanwise direction (See figure 7 in comparison to figure 5).

Between two consecutive Kármán vortices of the same sign, the magnitude of the streamwise vorticity varies. The maximum occurs close to the downstream Kármán vortex where the free stagnation point is located. Since the free stagnation points in the upper and lower layer are in a staggered configuration like the evolving Kármán vortices, the streamwise vorticity components at a given X-location grow at different rates in the upper and lower layer. Consequently, the interaction and the lateral displacement of the streamwise vortices evolving from each layer vary along the flow direction (X); and hence, we see unequal lateral displacement of the streamwise vortices as we move along the flow direction. This effect results in the formation of λ-shaped vortical structures (figure 8). This process clearly presents a manifestation of the three-dimensional interaction of the two layers of vorticity. The presence of one dominating sign of vorticity in plane mixing layers is the reason this effect was neither observed in the mixing layer numerical simulations (Ashurst & Meiburg 1988) nor in the experimental flow visualizations (Lasheras & Choi 1988).

The streamwise vorticity component experiences maximum amplification close to the free stagnation points. Consequently, the filaments located there show the largest wavy dislocation. Thus, within a layer, the formation of pairs of counter-rotating streamwise vortices is more pronounced closer to the core region than in the centre of the braids (in the downstream half of each braid). This becomes apparent at time

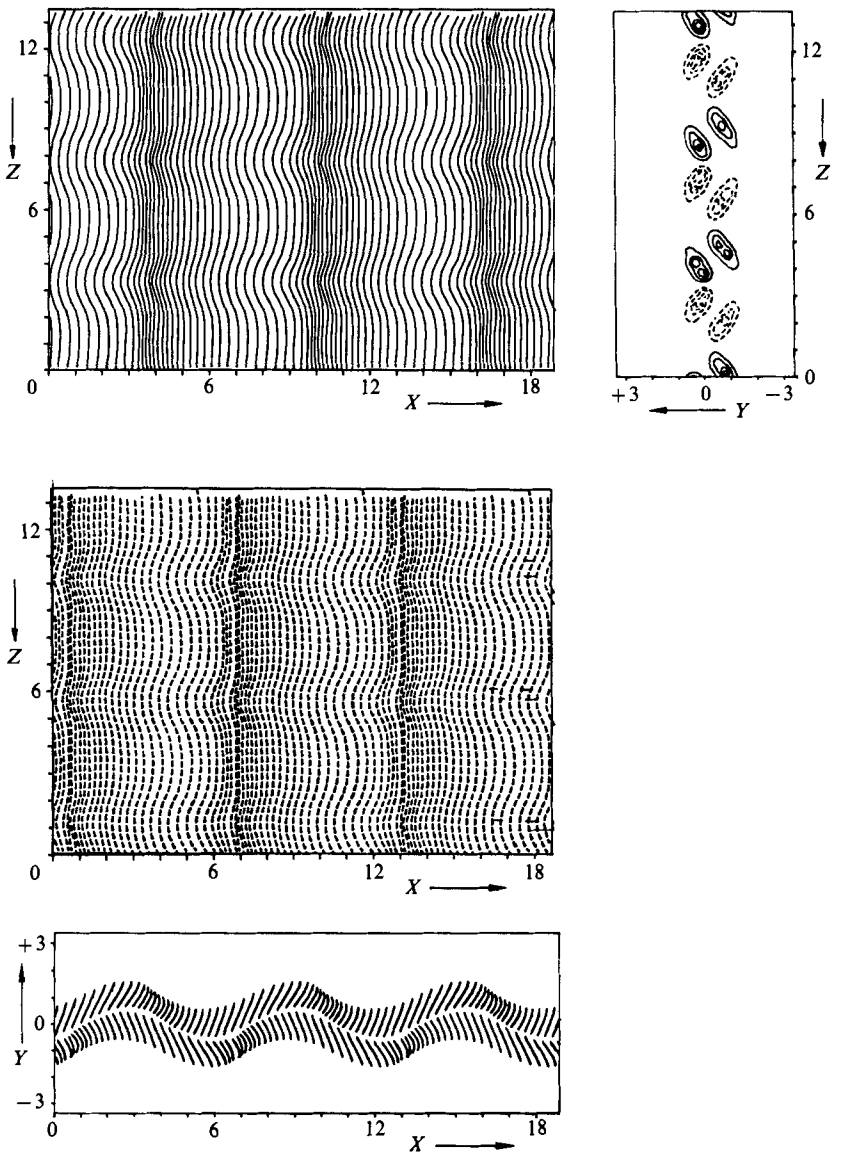

FIGURE 7. Top views of the filaments of the upper (solid lines) and lower (dashed lines) layers at time $t = 126.25$. The side view shows the integrated view of all the filaments of both the upper and lower layer. Constant streamwise vorticity contours at a distance $x = 4.6$ are also given.

$t = 126.25$ (figure 7) from the shapes of the filament centrelines, which just upstream of the core region have the form of rather short kinks joined by nearly straight lines, whereas the filaments in the central portion of the braids are shaped more like sine waves.

The plane of the evolving streamwise vortices becomes aligned with the principal plane of the two-dimensional strain field created by the spanwise rollers, and as a result, they form an angle with the plane of the wake (X, Z-plane), as shown in the side view for $t = 155$ (figure 8) and side view for $t = 169$ (figure 9). These λ-shaped structures strongly resemble the horseshoe vortices known to form in the plane boundary layer, a fact which is not surprising considering that the boundary layer

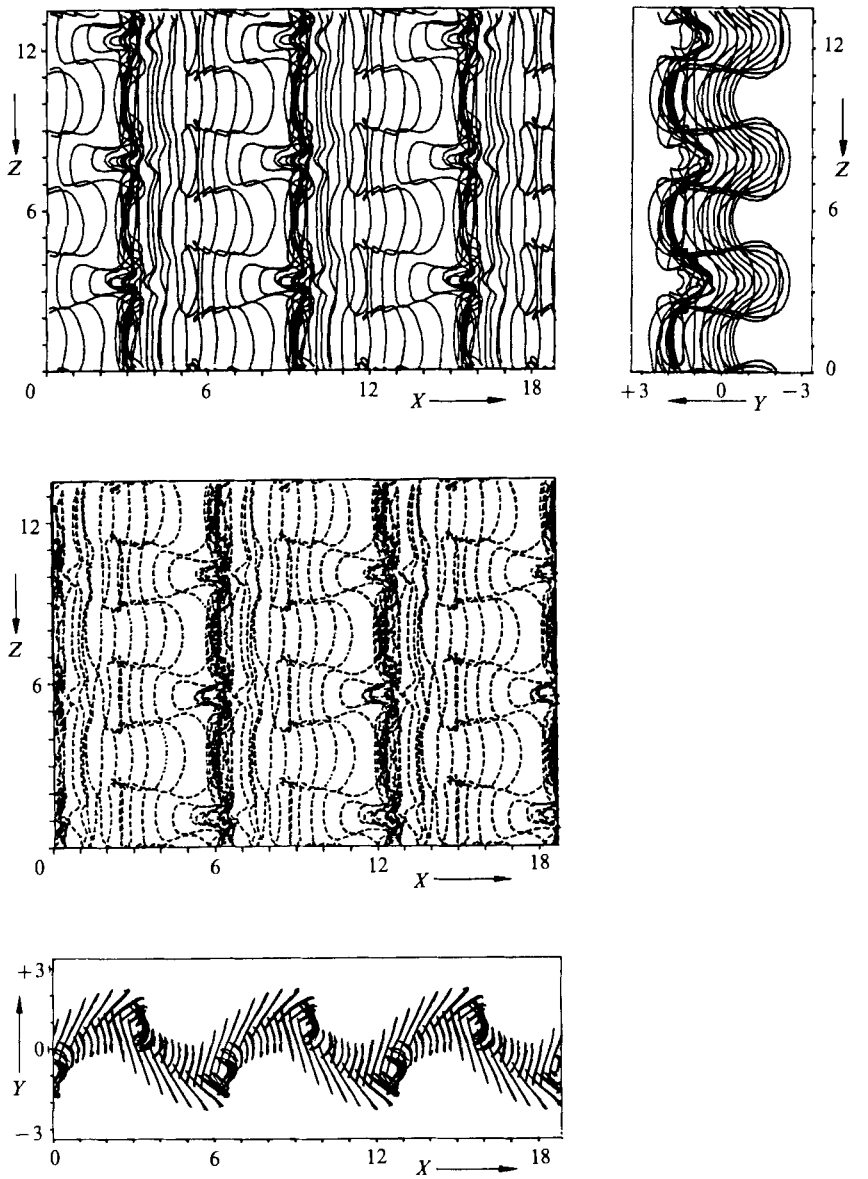

FIGURE 8. Top view of the filaments of the upper (solid lines) and lower (dashed lines) layers at time $t = 155$. The side view shows all the filaments of both the upper and lower layer. An end view of the filaments of the upper layer is also given, showing the wavy undulation caused in the spanwise vortices by the evolving streamwise structure.

can, in a sense, be viewed as a flow containing two opposite layers of vorticity with the wall representing the plane of symmetry. Similar structures have also been observed experimentally to exist in the braids of plane mixing layers developing behind a flat plate when the wake component is appreciable (Lasheras & Choi 1988, their figure 23*a*, *b*). Furthermore, recent computational results of Rogers, Moin and Reynolds (1986) on structures in homogeneous turbulent shear flows, indicated that

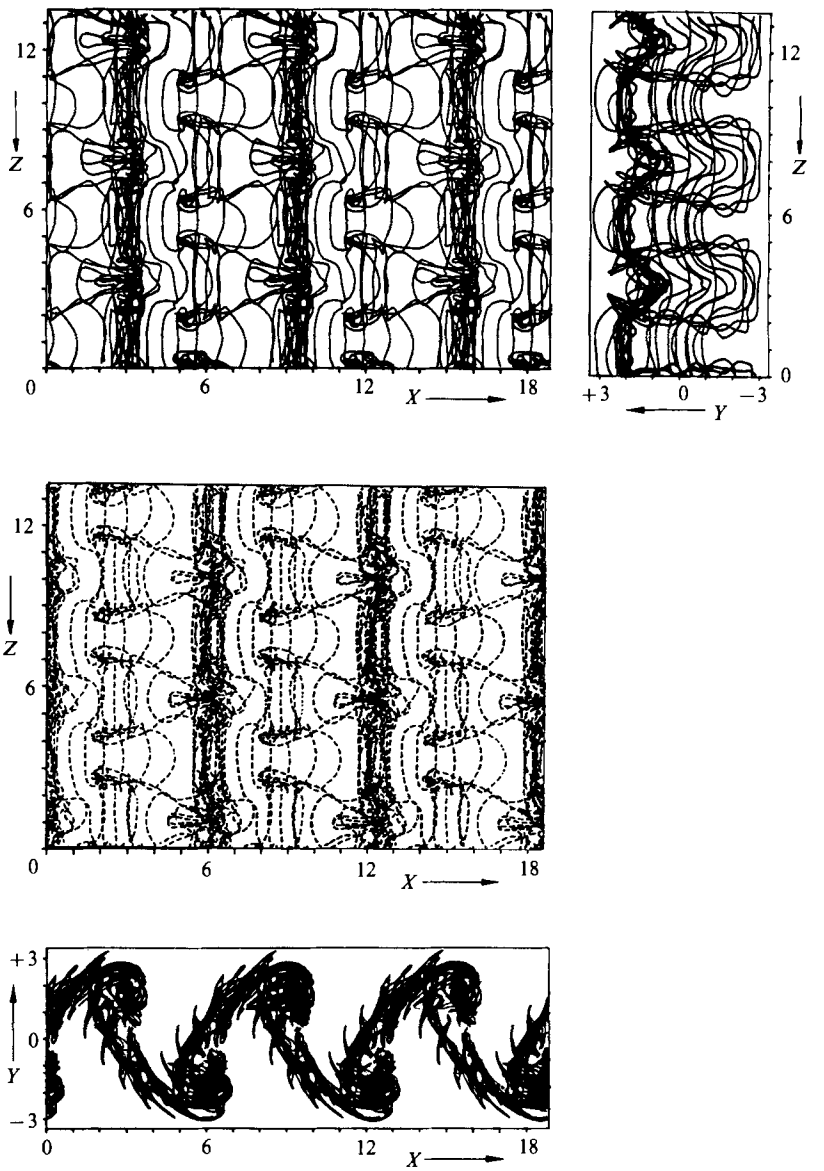

FIGURE 9. Top view of the filaments of the upper (solid lines) and lower (dashed lines) layers at time $t = 169$. The side view shows all the filaments of both the upper and lower layer. An end-view of the filaments of both the upper and lower layers is also given, showing the wavy undulation caused in the spanwise vortices by the evolving streamwise structure. Notice that the perturbed Kármán vortices of the upper and lower layer exhibit an in-phase vertical undulation.

the formation of these hairpin vortices in the presence of the global shear is a generic process to be found in many of these flows.

As the streamwise vortex tubes evolve, they interact with the spanwise vortices by lifting them up and pushing them down in an alternating fashion. The resulting curvature of the spanwise vortices, in turn, causes further stretching and intensification of the streamwise vorticity as can be seen in figure 9. Thus, the

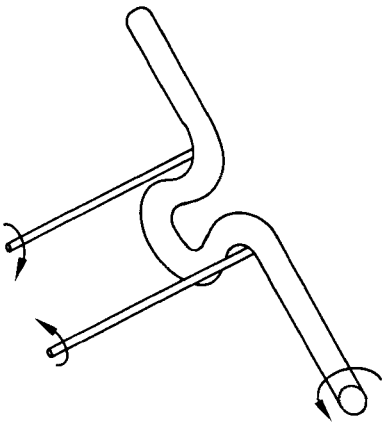

FIGURE 10. Sketch of the interaction of streamwise and spanwise vortices.

interaction between the streamwise and the spanwise vortices proceeds in a self-amplifying manner, as sketched in figure 10.

Three perspective views of the experimentally visualized and the numerically calculated position of the interface of the evolving three-dimensional plane wake are presented in figures 11, 12 and 13. In these perspective views, it is clearly visible how the interface wraps around both the evolving spanwise Kármán-like vortices and the streamwise ones. The interface visualization (figure 13) reveals how the spanwise vortices experience an undulation along the span caused by their interaction with the streamwise vortices, an effect also clearly observed in the numerical simulation (figure 9). Noticeable in the near-plan view (figure 11) is that as a result of the interaction between the streamwise vorticity components of each layer, the streamwise vortices do not point in the axial flow direction (X), but rather form a λ-like pattern. This is also apparent in the numerically simulated vorticity configuration (top view of figure 8). From the near-side view (figure 12), it is seen how under the effect of the strain field created by the evolving spanwise vortices, the streamwise vortices orient themselves in directions inclined to the plane of the wake (plane X, Z). This observed alignment of the streamwise vortex tubes along the principal axis of the two-dimensional strain field created by the spanwise rollers was also shown in the vortex dynamics simulation (side view of figure 9).

The close agreement between the experimental and the numerically calculated interfaces suggests that for this laminar wake, evolving from two laminar boundary layers, inviscid vortex dynamic methods are able to correctly reproduce the mechanisms of concentration and stretching of the vorticity. Furthermore, these inviscid vortex induction mechanisms appear to be the dominant ones in the initiation of the three-dimensional development of the plane wake.

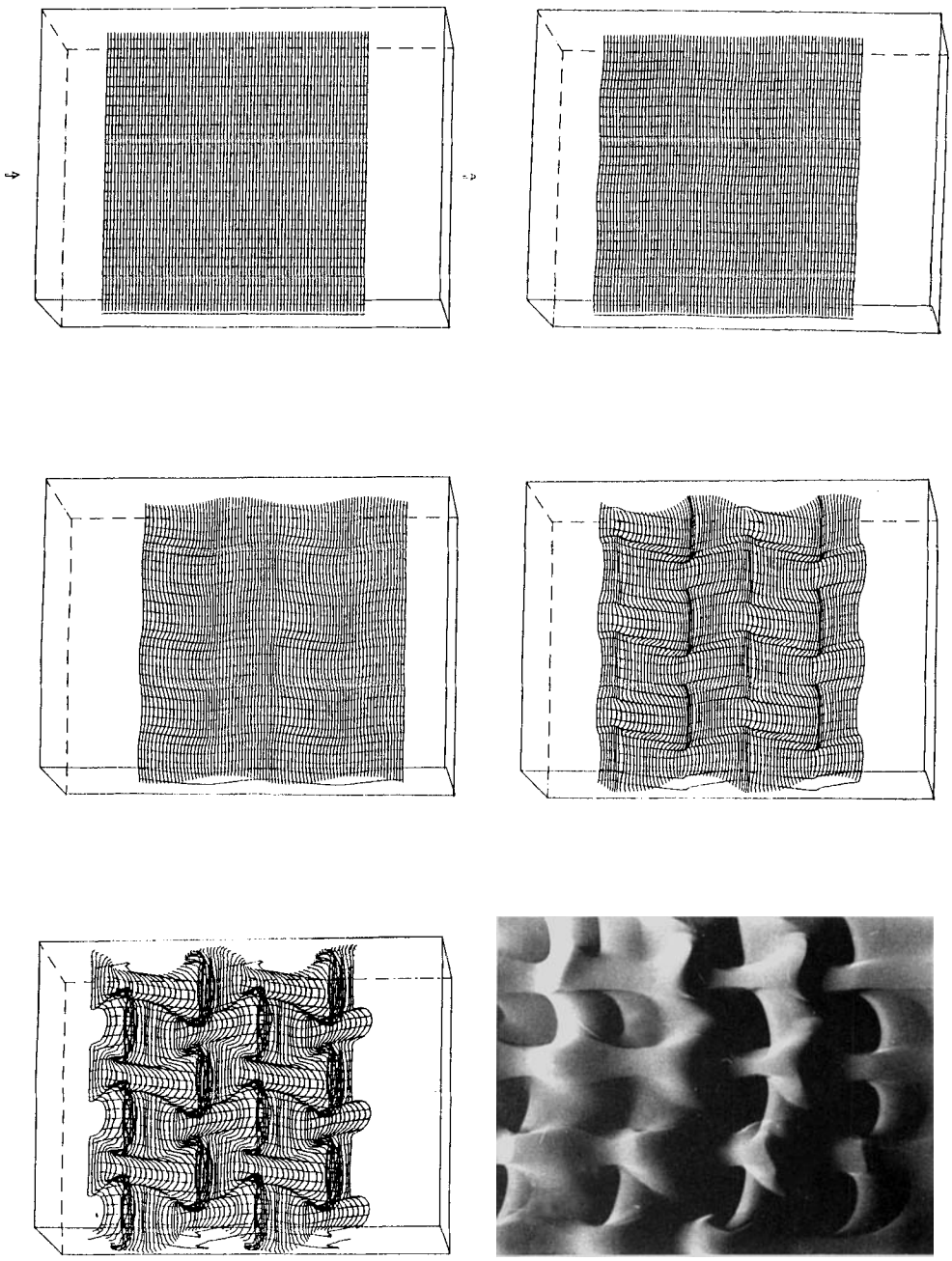

FIGURE 11. Near-plan perspective view of the numerically calculated time evolution of the interface separating both sides of the wake. The experimentally obtained interface visualization from the same perspective angle is also shown.

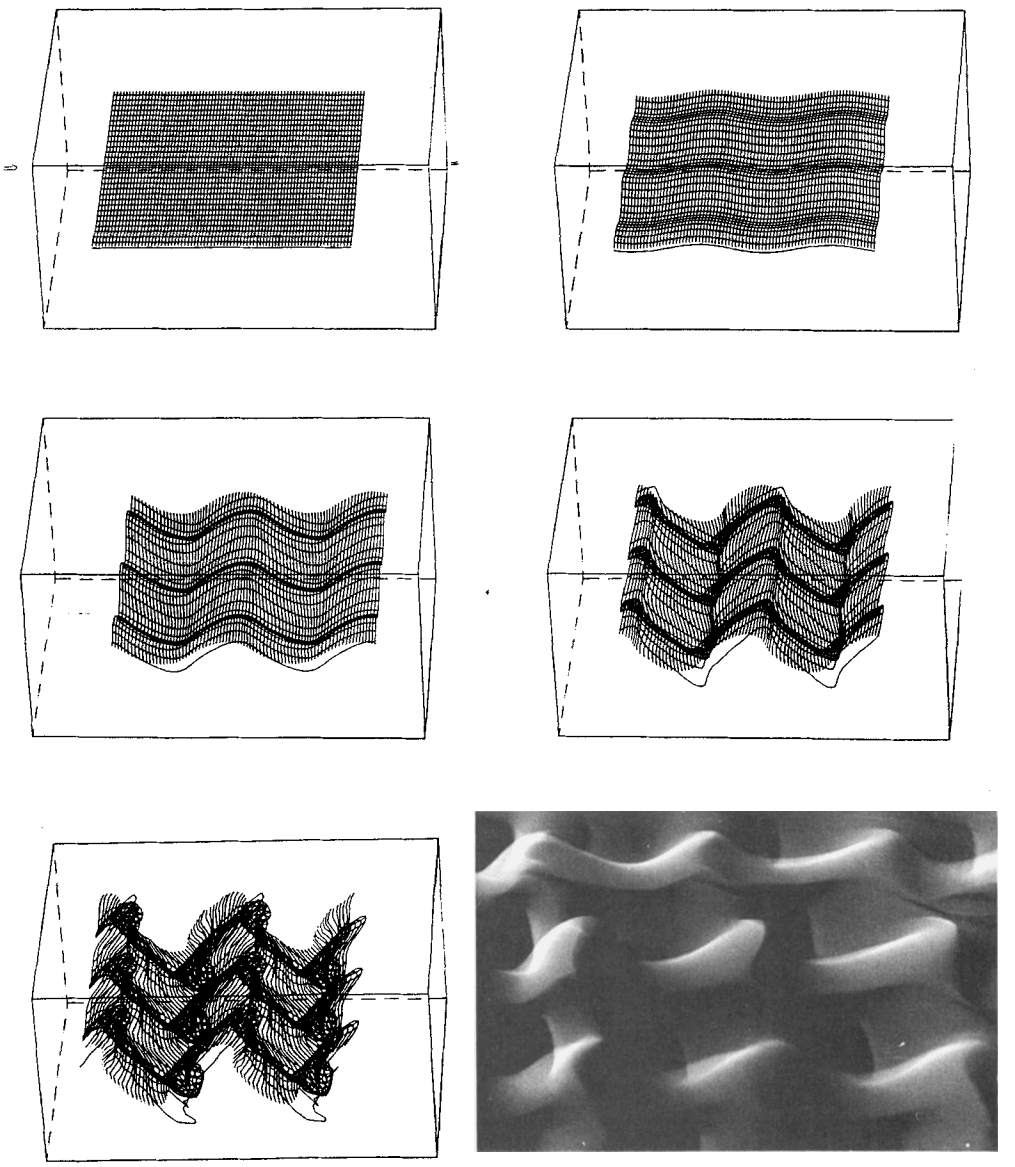

FIGURE 12. Near-side perspective view of the numerically calculated time evolution of the interface separating both sides of the wake. The experimentally obtained interface visualization from the same perspective angle is also shown. The spanwise variation in the strength of the Kármán vortex is apparent from the interface roll-ups.

5. Mechanism for the three-dimensional transition, effect of a vertical perturbation

The experimentally observed and numerically calculated three-dimensional evolution of the flow can be described schematically in the following sequence. The two-dimensional shear instability leads to the formation of concentrated vorticity in two staggered rows, i.e. the Kármán vortex street. These evolving spanwise vortices create strain fields between them. In a reference frame moving with the average

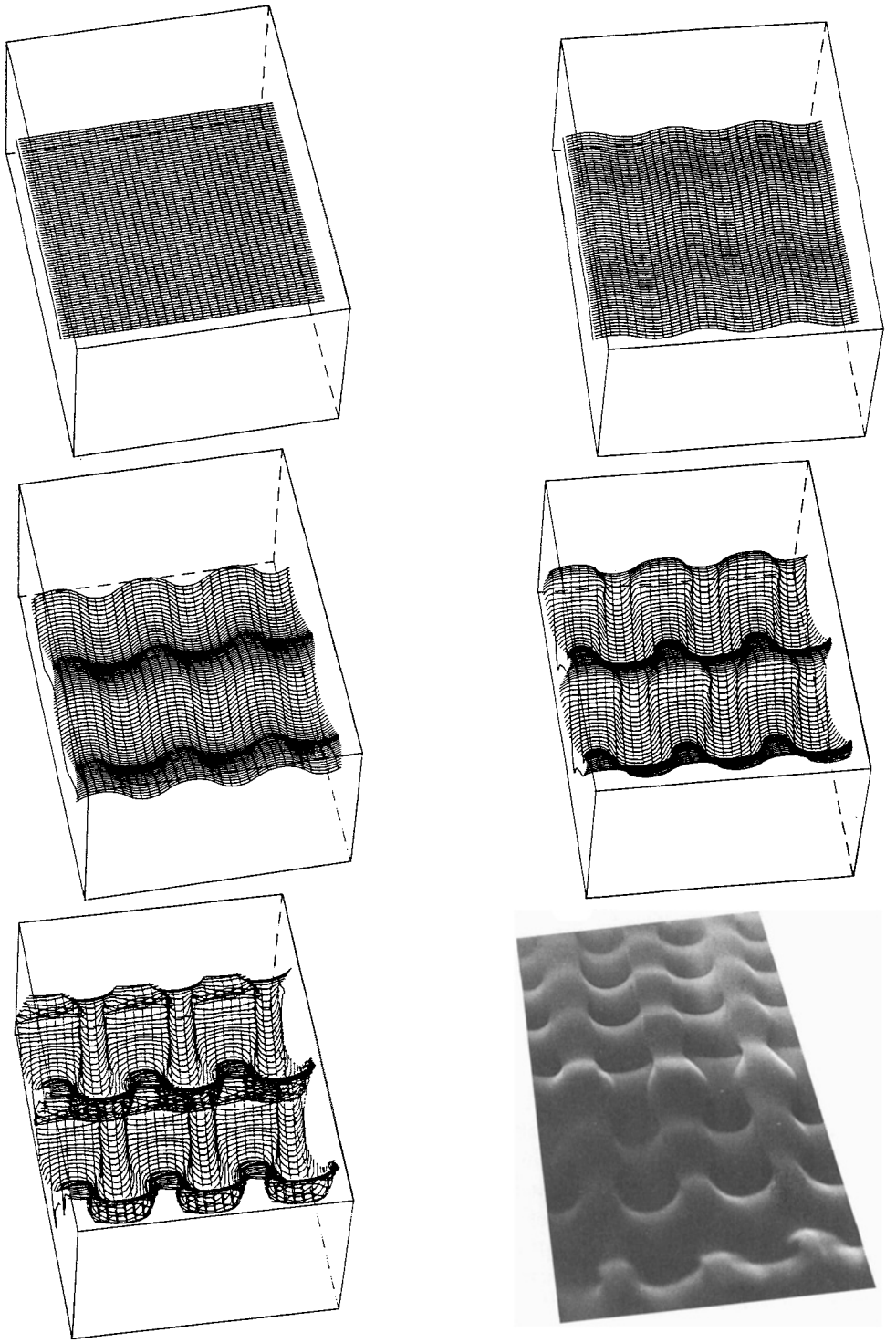

FIGURE 13. Near-end perspective view of the numerically calculated time evolution of the interface separating both sides of the wake. The experimentally obtained interface visualization from the same perspective angle is also shown. Observe the vertical undulation of the Kármán vortices caused by the streamwise structure. Notice the equal rotation sense of the axial vortices on the braids connecting two consecutive Kármán vortices.

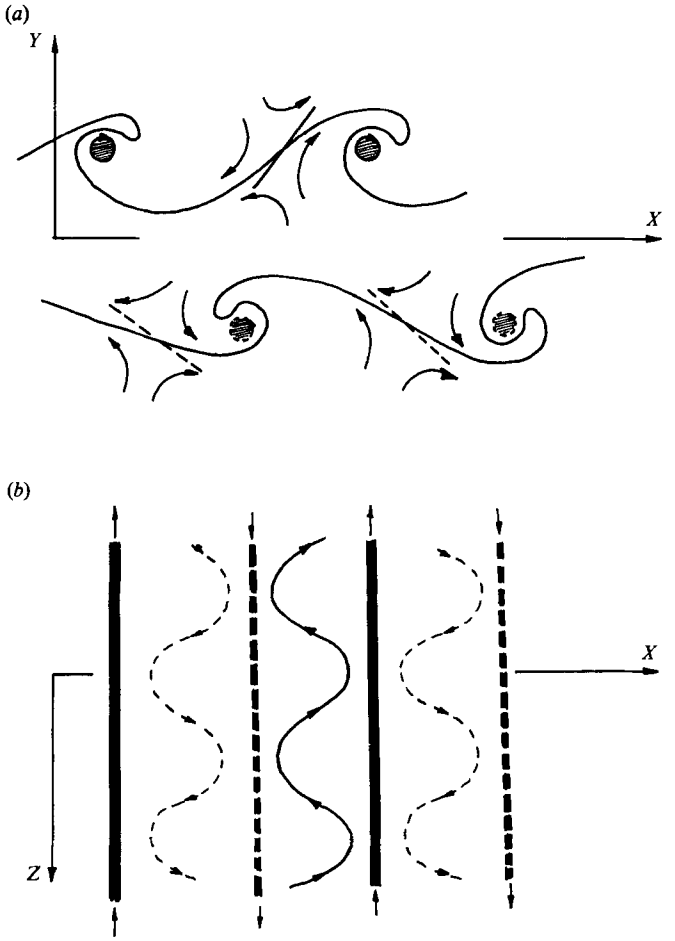

FIGURE 14. Evolution of the vorticity field under the effect of a vertical perturbation, (*a*) Schematic representation of the side view of the wake showing the location of the free stagnation points in each layer. The perturbed vortex lines of each layer are tilted in the direction of the principal planes of strain acquiring a 180° out-of-phase undulation shown in the plan view. (*b*).

velocity of these rollers, the strain field develops the qualitative configuration schematically sketched in figure 14(*a*). Under the effect of the shear, the vertical loops of the perturbed vortex lines existing in the braids tilt into the horizontal, streamwise direction, while simultaneously being stretched. This process eventually results in the reorientation of the vortex lines in the braids of both layers into the direction of the principal planes of strain created by the evolving spanwise rollers. Because of the different signs of the vertical shear in each layer, the tilted vortex filaments of the lower layer acquire a 180° phase shift with respect to the ones in the upper layer. Notice that the vortex filaments of the upper layer rotate clockwise tilting into the streamwise direction while the ones of the lower layer rotate counterclockwise (figure 14*b*), For simplicity only one filament has been sketched in each braid region of both layers. Due to the presence of the vortex of opposite sign, the location of the free stagnation points in the upper and lower layers are displaced towards the downstream vortices. Thus, the deformed vortex loops close to the stagnation point begin wrapping around the downstream Kármán vortex, in this

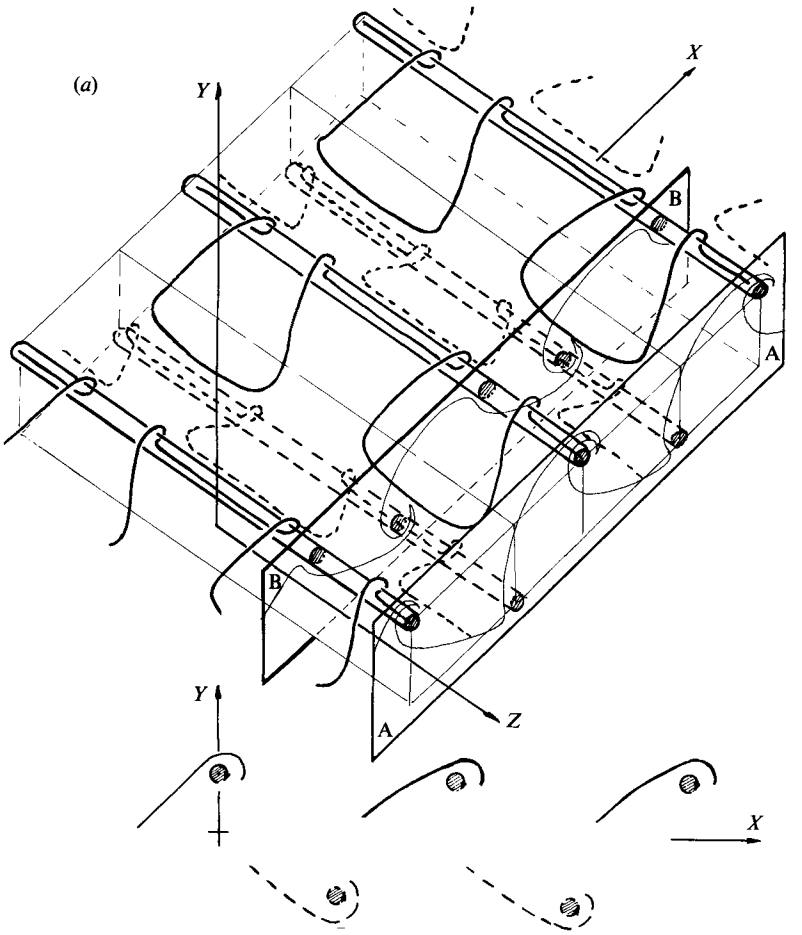

FIGURE 15(*a*). For caption see next page.

way adding vorticity of the same sign periodically along the span (figure 15). Simultaneously, the interaction of the evolving streamwise vorticity of the upper and lower layer causes the stretched vortex lines in each layer to acquire a λ shape, rather than to point in the flow direction (X) (figure 15*a*).

At this stage, the stretching and concentration of vorticity have already caused a break in the vertical symmetry of the wake. The half-wavelength shift in the spanwise direction between the vortex lines of the braids of both layers is responsible for this loss of symmetry. Notice that a vertical cross-cut (plane parallel to XY) along section A–A in figure 15*a* reveals that at this location, the Kármán vortex of the upper layer has become stronger than that in the lower layer. However, because of the 180° phase shift between the perturbed vortex lines of the two layers, a cross-cut along section B–B (a half wavelength from A–A) shows the reverse effect, i.e. the strength of the Kármán vortex in the lower layer has now become greater than that in the upper layer. Flow visualizations of these vertical cross-sections obtained using laser induced fluorescence show precisely the above described, non-symmetric vorticity configuration (figure 16). The perspective view of the interface given in figure 17 also reveals its non-symmetric shape. Notice in this figure that the roll-up of the interface is more pronounced at positions where the circulation of the Kármán

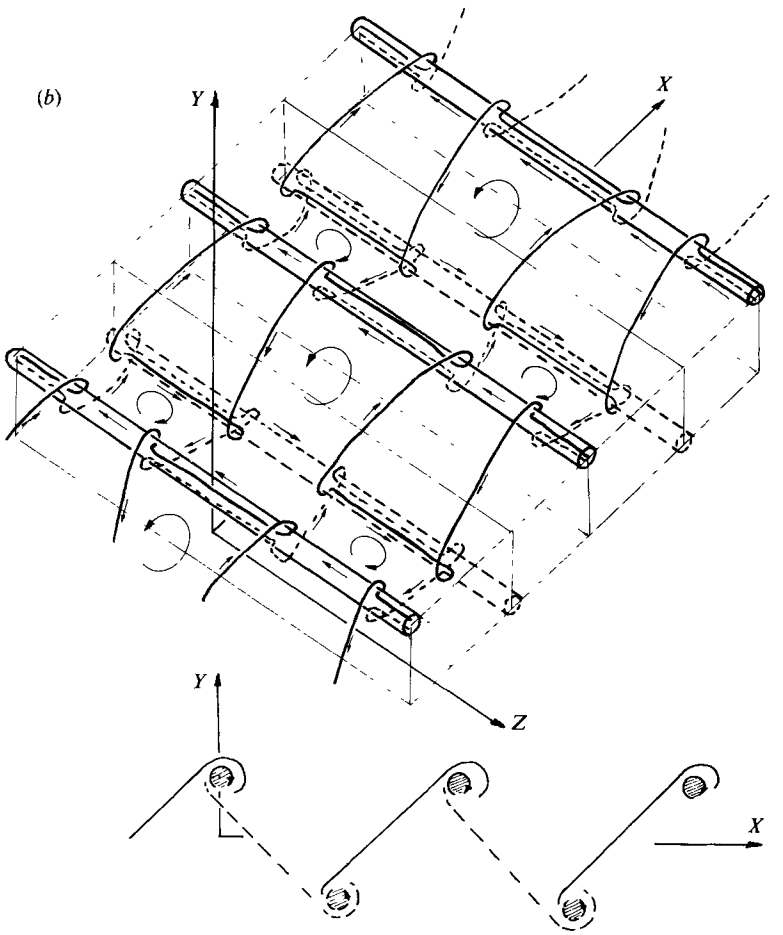

FIGURE 15. Perspective view of the three-dimensional evolution of the vorticity field resulting from a vertical perturbation. (*a*) The vortex filaments of each layer located in the stagnation region experience the maximum amplification. The stretched filaments wrap first around the downstream Kármán vortices causing an increase in their circulation periodically along the span. The 180° phase shift between the two layers causes a break of symmetry. (*b*) Vorticity configuration achieved after the formation of the Kármán vortex street.

vortices is greater. The vertical cross-cuts of the interface (figure 17*b*) show the alternating fashion in which circulation of the same sign is added to the Kármán vortices of each layer, thus leading to a non-symmetric pattern of the strength of the upper and lower Kármán vortices.

As the streamwise vortices evolving in the upper and lower layers interact with the nearest, downstream, two-dimensional Kármán vortices, they cause an undulation in the spanwise vortices. Under this effect, the Kármán vortices of both layers achieve undulations of wavelengths equal to the wavelength of the initial perturbation. However, because of the 180° phase shift between the positive and negative vorticity observed for this flow, the cores of the Kármán vortices of the upper layer acquire an undulation in phase with the undulations of the vortices of the lower layer. Laser induced fluorescence and flow visualizations of vertical cross-cuts of the wake reveal this wavy undulation in the Kármán vortices of both the upper and lower layer (figure 18). Noticeable from these near-end view cross-cuts is that the undulations in

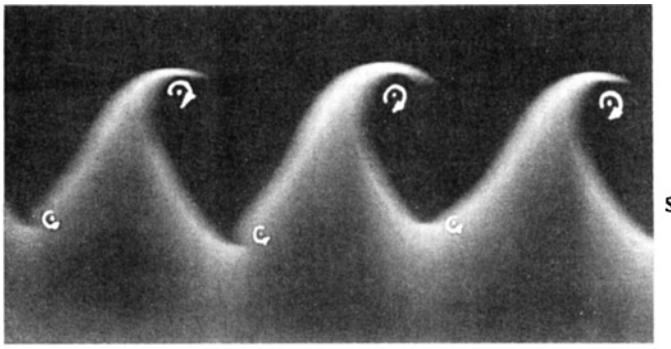

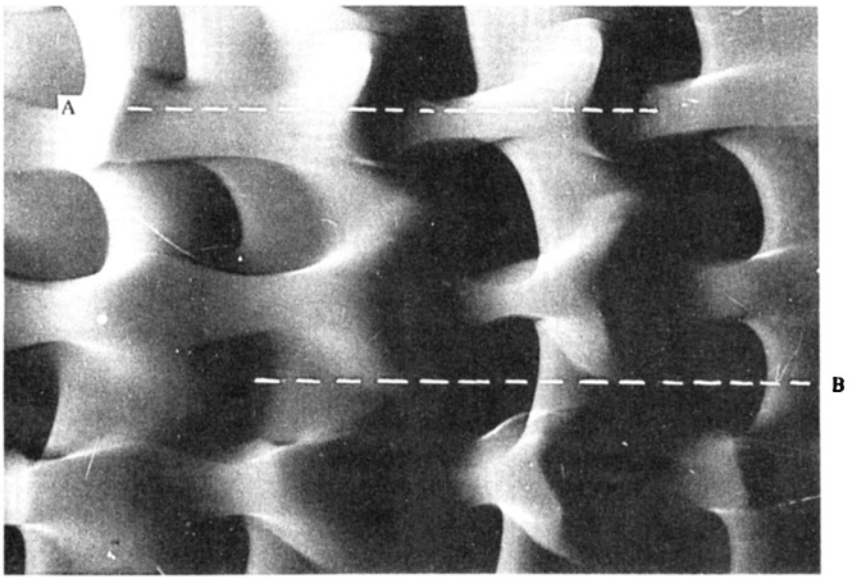

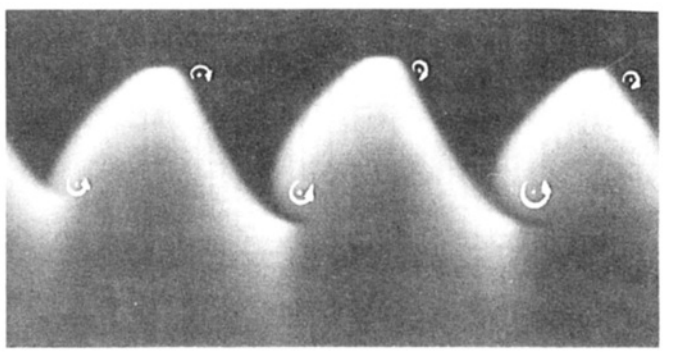

FIGURE 16. Effect of the vertical perturbation. Plan view of the interface separating both sides of the wake. The non-symmetric structure of the vorticity field is shown in the two LIF vertical (plane parallel to (X, Y) plane) cross-cuts (section A–A is 1 and $\frac{1}{2}$ wavelength from B–B).

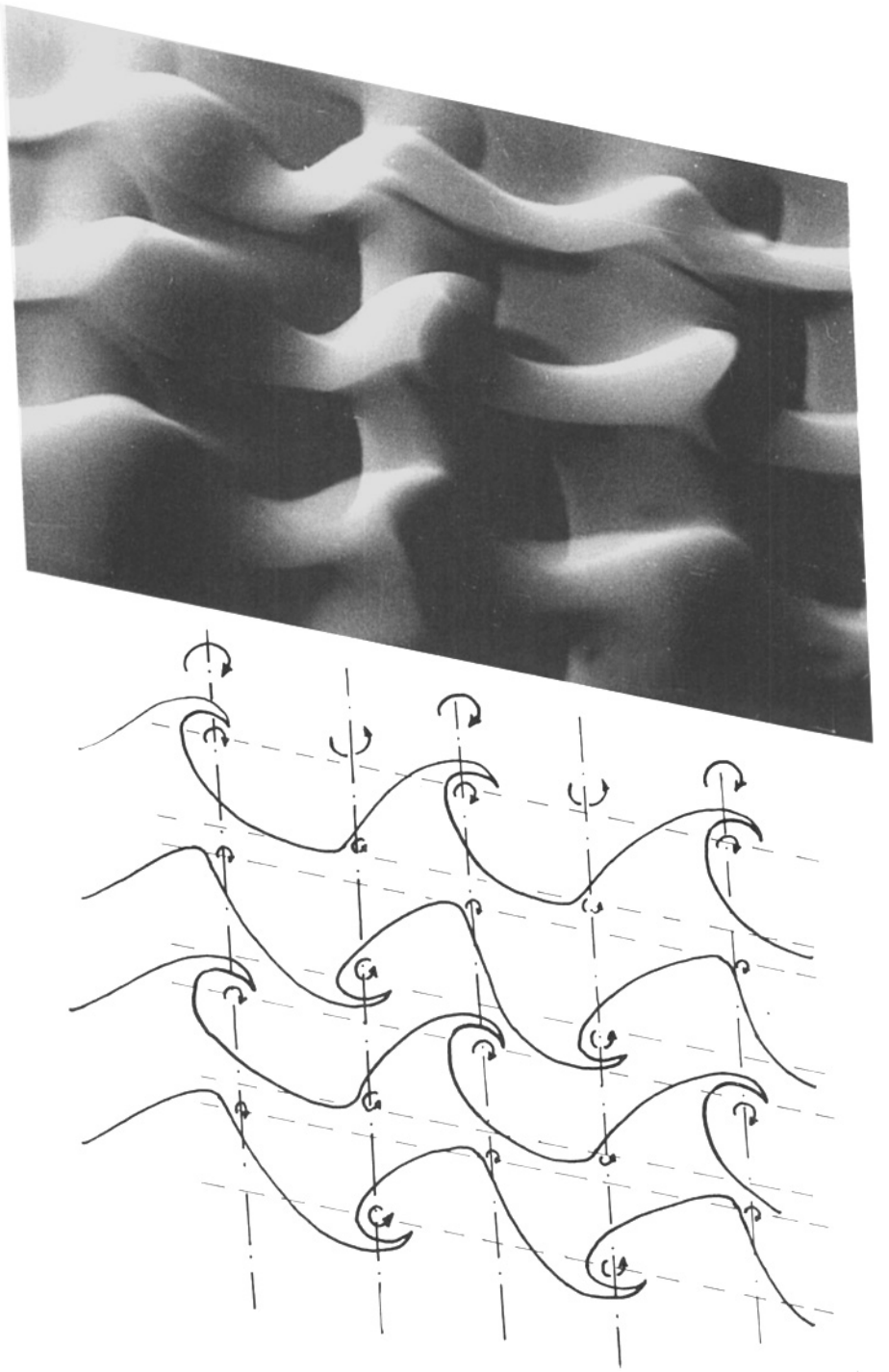

FIGURE 17. Effect of the vertical perturbation. Perspective view of the interface showing the non-symmetric structure of the wake.

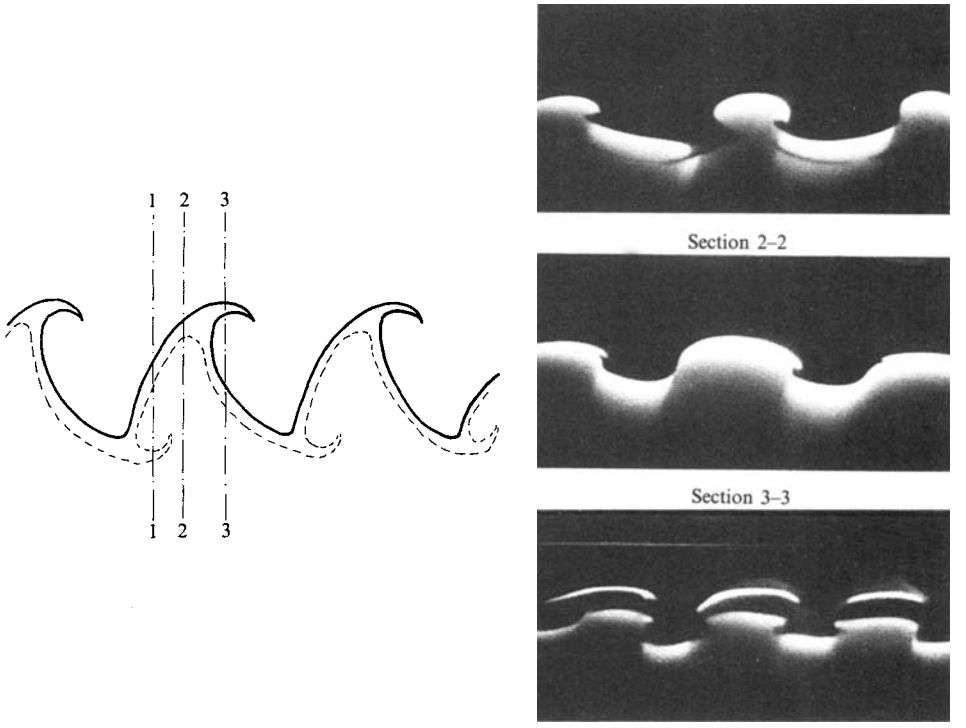

FIGURE 18. Effect of the vertical perturbation. Near-end views of LIF vertical cross-cuts (planes parallel to (Y, Z) plane). Observe that the undulation of the spanwise vortices of opposite sign is in-phase. Notice also the equal rotation sense of the streamwise vortices in the two consecutive braids.

the cores of the positive and negative Kármán vortices are in phase with each other.

As the vorticity of the two layers further concentrates in Kármán-like vortices, the orientation of the principal plane of positive strain created by these two-dimensional vortices continues to become more inclined with respect to the plane of the wake. The principal planes of positive strain rotate counterclockwise and clockwise in the upper and lower layers, respectively (figure 15*b*). During this reorientation, the streamwise vortex lines begin to experience stretching by the Kármán vortex of the opposite layer until they eventually wrap around them. This strong interaction between the two layers of vorticity leads to the configuration of the vorticity field shown schematically in figure 15(*b*). Notice that the principal planes of positive strain now connect consecutive Kármán vortices of opposite sign. The topological structure of the vorticity field achieved at this point shows the possibility of a relinking of vortex lines to form closed vortex loops in the braids connecting two consecutive spanwise vortices of alternating sign. These closed vortex loops are not caused by the bending of one vortex line into a loop, but rather they appear in the overall vorticity configuration. A topological change leading to the formation of closed vortex loops was suggested by Roshko (1976) as a possible structure compatible with Grant's correlation measurements. However, a detailed mechanism for their formation has not been proposed until now.

A schematic representation of the structure of the vorticity field achieved at this

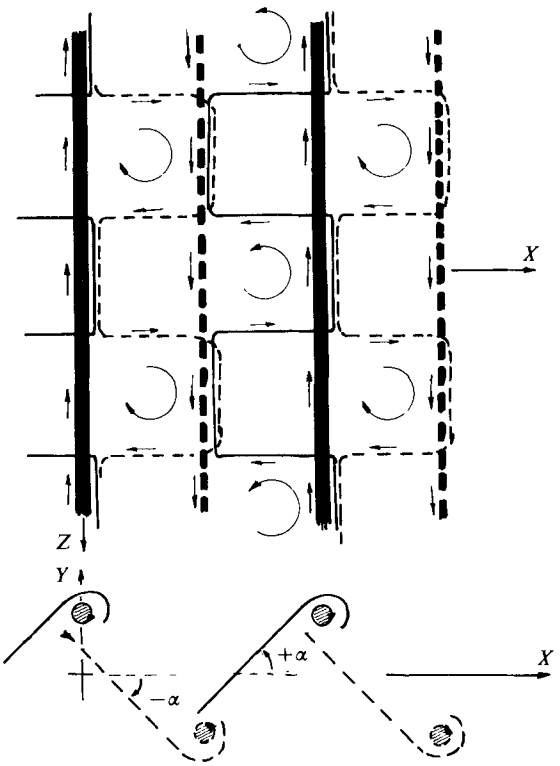

FIGURE 19. Schematic representation of the vorticity field resulting from the vertical perturbation. Observe the existence of a staggered array of closed vortex loops in the topological structure of vorticity field.

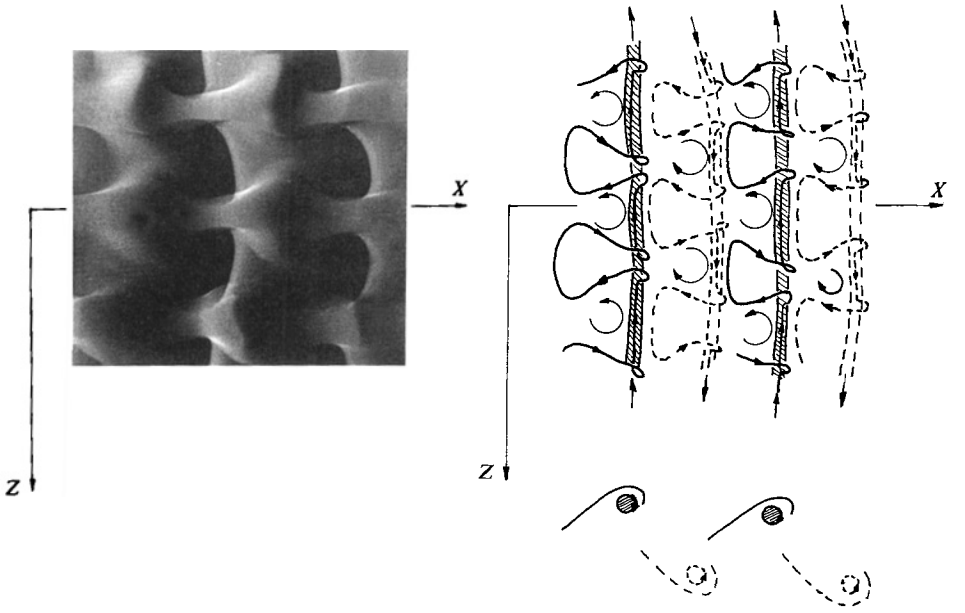

FIGURE 20. Effect of the vertical perturbation. Plan view of the interface separating the two sides of the wake. A sketch of the corresponding vorticity configuration showing the staggered array of closed vortex loops is also given.

point is given in figure 19. Observe that the rotation in the orientation of the principal plane of positive strain in each layer has led to the formation of closed vortex loops in planes inclined $+\alpha$ or $-\alpha$ to the plane of the wake XZ. Their sign and position along the span alternate by half a wavelength between two consecutive principal planes of positive strain. In each plane, the closed vortex loops are all of the same sign and they are located one full wavelength apart from each other along the span.

The position and sign of these closed vortex loops are reflected in the plan view of the interface flow visualization (figure 20). For illustrative purposes, a sketch of the corresponding vorticity field showing the organization of the stretched vortex lines which have led to this flow configuration is given in figure 20(*b*).

6. Effect of the initial conditions

After having analysed the case corresponding to a vertical perturbation sinusoidally distributed along the span, in this section we will first study the response of the base-flow to a periodic, horizontal perturbation. Following this analysis we will study the combined effect of vertical and horizontal perturbations of the same wavelength.

6.1. *Horizontal perturbation*: *development of the three-dimensional structure*

The horizontal perturbation was produced by an indentation of amplitude a and wavelength λ in an otherwise flat splitter plate. The amplitude was 6 mm, while the wavelength was kept at $\frac{2}{3}$ of the most unstable Kármán street wavelength (as in the corrugated plate case).

The three-dimensional evolution of the flow which developed from this horizontal perturbation can be summarized as follows. Similar to the corrugated-plate case discussed above, the two-dimensional shear instability leads first to the concentration of spanwise vorticity in two staggered rows, i.e. the Kármán vortex street. These evolving spanwise vortices create strain fields in whose principal planes of positive strain the perturbed vortex lines lie (figure 21). Under the effect of these strain fields, the vortex lines become stretched in the streamwise direction. Because initially and throughout the stretching process the perturbed vortex lines are oriented in the direction of the evolving planes of positive strain, they will remain in phase with each other (in contrast with the 180° out-of-phase configuration observed in the case of the vertical perturbation). As the vorticity continues to concentrate in the Kármán vortices thereby depleting the braids of vorticity, the orientations of the principal planes of positive strain begin to rotate from the horizontal position counterclockwise and clockwise in the upper and lower layers, respectively. Because of the presence of the Kármán vortex of opposite sign, the stagnation point in each layer is closer to the downstream vortex (as in the case of the corrugated plate). The perturbed vortex lines of each layer then begin to wrap around the downstream Kármán vortex of the same sign. The vorticity field achieved at this point is schematically represented in figure 22(*a*). Observe that the stretching and concentration of vorticity has now preserved the symmetry of the plane wake. Although the circulation of the Kármán vortices of the upper and lower layers varies periodically along the span, vertical cross-cuts along planes parallel to the (X, Y)-plane reveal a symmetric configuration. A vertical cross-cut along section A–A in figure 22(*a*) shows that the strengths of the Kármán vortices of the upper and lower layers are equal at that location. Similarly, a cross-cut along section B–B (a half wavelength apart) shows the same effect, i.e.

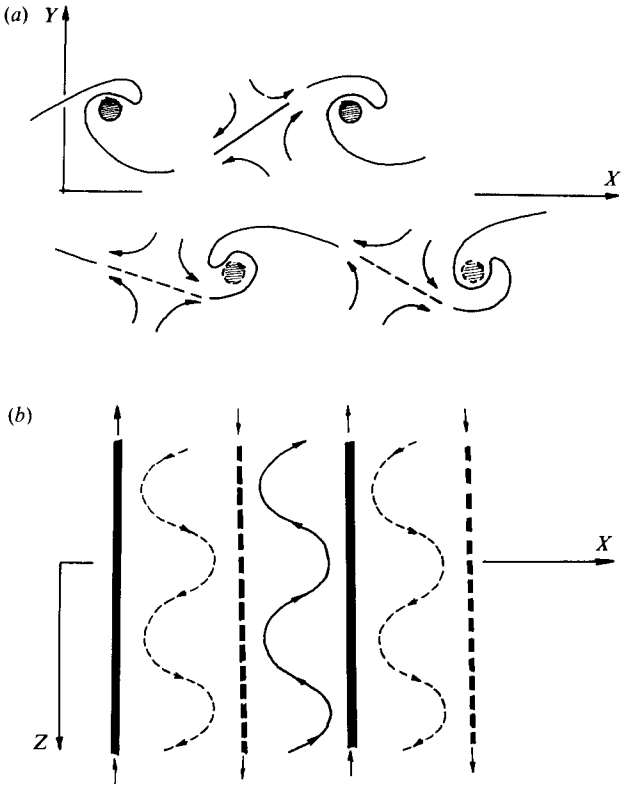

FIGURE 21. Evolution of the vorticity field under the effect of the horizontal perturbation. Schematic representation of the wake showing the location of the free stagnation points in each layer. The perturbed vortex lines are initially and throughout the stretching always oriented along the direction of the principal plane of positive strain. Thus the vortex filaments of each layer remain in-phase.

equal strengths of vorticity in the lower and upper layers. However, notice that the spanwise vortices are weaker in section B–B than in A–A. The fact that both layers of perturbed vorticity have remained in phase throughout the stretching process is now the cause of this preservation of the symmetry of the wake. Flow visualizations of cross-sections obtained using laser induced fluorescence (figure 23) show precisely the above described symmetry. Figure 23 (*a*) corresponds to cross-section A–A, while figure 23 (*b*) corresponds to cross-section B–B. Notice that the addition of circulation of the same sign at the same spanwise location in both the upper and lower layer has resulted in a periodic strengthening of the Kármán vortices along the span. However, equal strengths are observed in the upper and lower layer at each section.

As the evolution of the wake continues and the orientation of the principal plane of positive strain continues to rotate, a strong strain field develops between consecutive, spanwise vortices of opposite sign. The stretching and subsequent re-orientation of the vorticity of the braids now lead to the configuration schematically shown in figure 22 (*b*). As the perturbed vortex lines wrap around consecutive Kármán vortices of opposite sign, the topological structure of the vorticity field achieved at this point again shows the existence of closed vortex loops. However, observe now that the closed vortex loops of alternating sign are all aligned in the flow (x) direction, (figure 24). Notice that, as was the case with the vertical perturbation

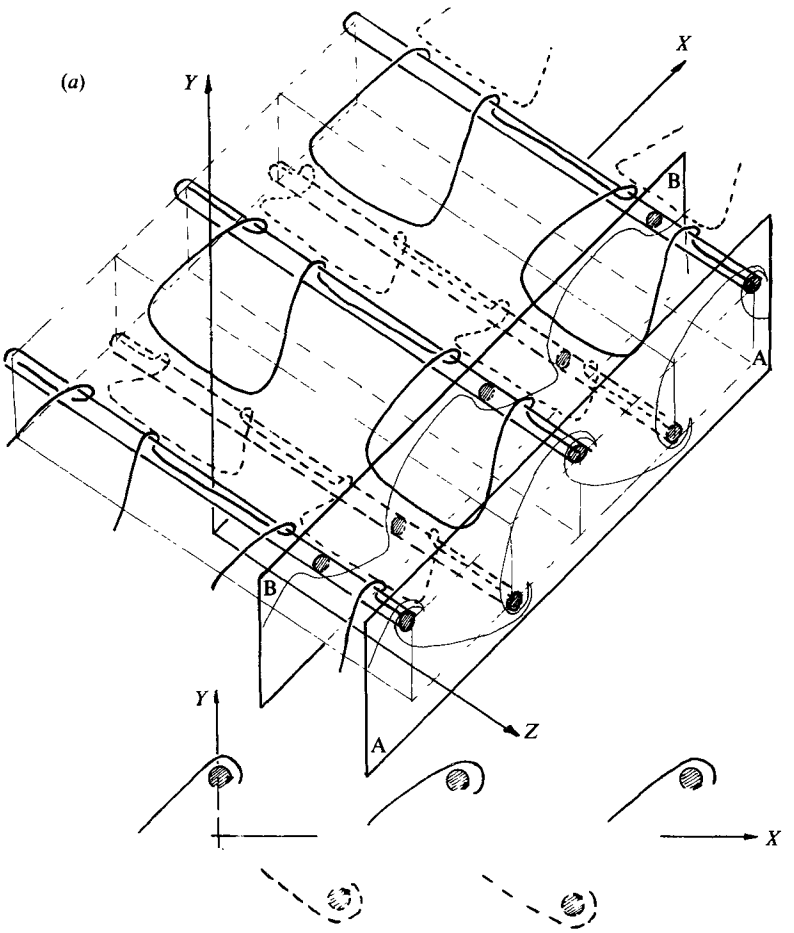

FIGURE 22(*a*). For caption see next page.

(corrugated plate), these closed vortex loops are also one full wavelength apart in the spanwise direction, and that their signs alternate between consecutive planes of strain (braids).

The location and sign of these closed vortex loops are visible in the plan view interface flow visualization (figure 25) as well as in the near-end perspective view interface visualization (figure 26). For illustrative purposes, a sketch of the corresponding vortex lines is given in figures 25 and 26. At this point it is important to mention that the configuration of the three-dimensional wake (figure 24) differs substantially from the one developed from the vertical perturbation (figure 19). The most important difference is that the horizontal perturbation preserves the symmetry of the wake while the vertical one leads to a loss of its symmetry. Thus, two different topologies of the three-dimensional vorticity field result from the perturbations, a symmetric one showing closed vortex loops in the braids aligned in the flow direction, and a non-symmetric one showing a staggered array of closed vortex loops in the braids of the Kármán vortex structure.

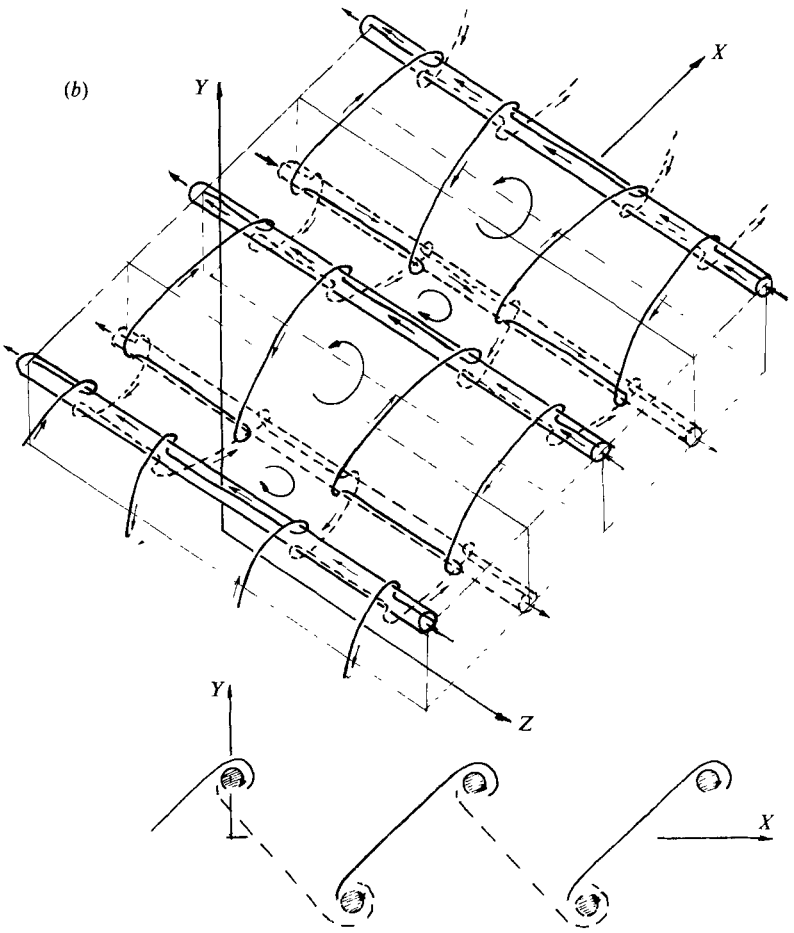

FIGURE 22. Perspective view of the three-dimensional evolution of the vorticity field resulting from a horizontal perturbation. (*a*) The stretched filaments of each layer wrap first around the downstream Kármán vortices causing an increase in their circulation periodically along the span. Because the perturbed vortex filaments of both layers are in-phase, the wake preserves its symmetry. (*b*) Vorticity configuration achieved after the formation of the Kármán vortex street.

6.2. *Effect of a perturbation with both vertical and horizontal components*

After having studied the effect of a single perturbation and having found that each perturbation mode leads to a distinct three-dimensional configuration of the vorticity field, we will now analyse the response of the plane wake to combined horizontal and vertical perturbations. We have limited our study to only those cases where the perturbations are either in-phase or 180° out-of-phase. Previous experiments on plane free shear layers (Lasheras & Choi 1988) have qualitatively shown that during the initial evolution the effect of both perturbations can be linearly superimposed. Therefore, it was expected that a similar linear behaviour could also occur in the wake.

When the wake flow was subjected to both vertical and horizontal perturbations in phase with one another (the peaks of the corrugations in phase with the tips of the indentations of the plate) our flow visualization revealed that depending on the

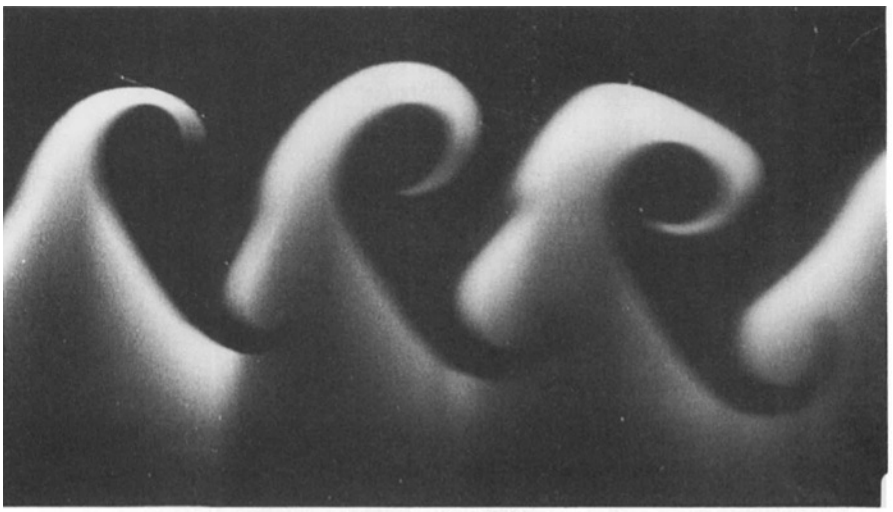

Section A–A

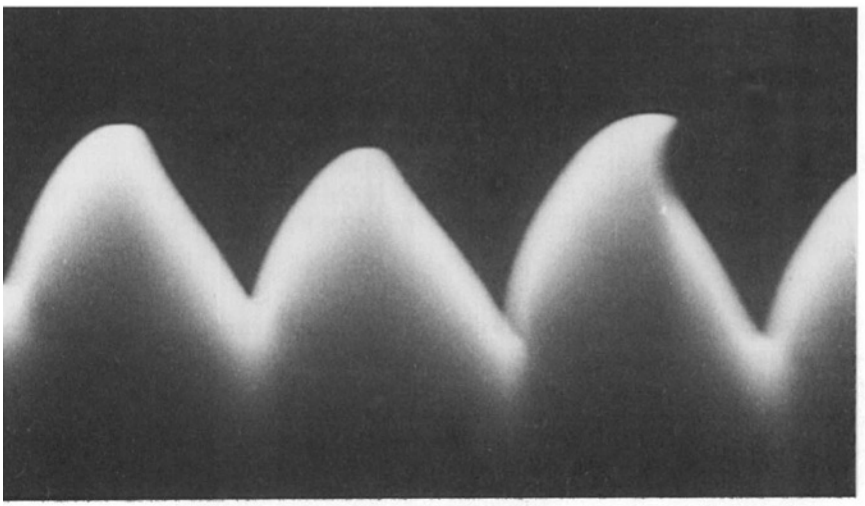

Section B–B

FIGURE 23. Effect of the horizontal perturbation. The symmetry of the wake is shown in the LIF cross-cuts (section A–A is a half wavelength from section B–B).

relative magnitude of each component, the vorticity field developed a configuration similar to either the one corresponding to a single vertical perturbation (figure 19) or the one resulting from a single horizontal perturbation (figure 24). When the amplitude of the vertical perturbation (corrugation) was very small with respect to the amplitude of the horizontal one (indentation), the flow was observed acquiring the vorticity configuration given in figure 24. The tilting of the vertical perturbation into the principal planes of positive strain leads to an in-phase addition of both perturbations in the upper layer, while in the lower layer it results in a 180° out-of-phase superposition. Thus, the perturbed vortex lines of the upper layer acquire a very amplified, wavy dislocation while the ones in the lower layer show a much less

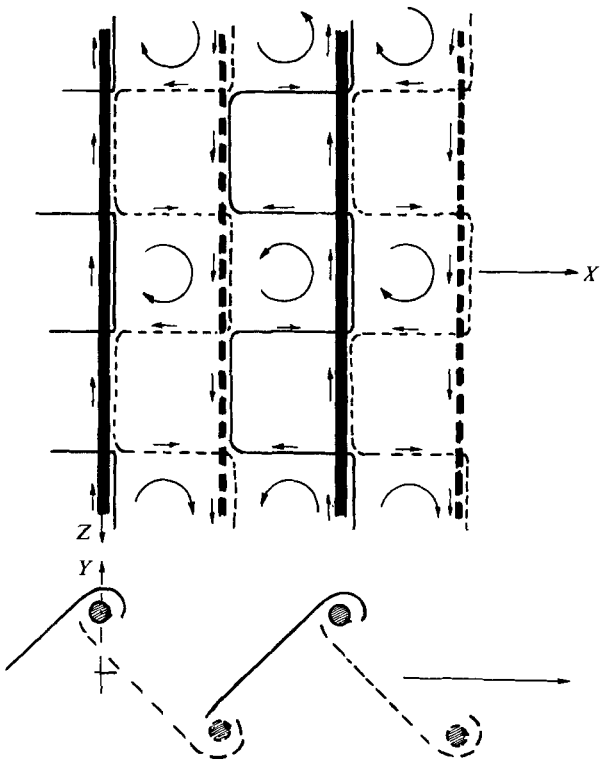

FIGURE 24. Schematic representation of the vorticity field resulting from a horizontal perturbation. Observe the existence of an array of close vortex loops in the topological structure of the vorticity field. In contrast with figure 19, notice that now, the alternating sign vortex loops are all aligned in the flow direction (X).

amplified in-phase dislocation. This is due to the partial cancellation caused by the reoriented vertical perturbation. The only remarkable difference between the purely horizontal perturbation and this case is the above mentioned unequal strength of the streamwise vortices in each braid. In addition, due to the much weaker interaction of the vortices in the lower layer with the ones in the upper layer (the streamwise vorticity component of the lower layer is very small) these vortices exhibit a much more pronounced orientation in the flow direction.

On the other hand, when the amplitude of the corrugation was increased to a large value, the wake was observed developing the vorticity configuration corresponding to a single vertical perturbation (figure 19). As the vertical perturbation reorients in both layers, its effect in the lower one cancels out the horizontal perturbation, and in addition, causes a reverse in its sign leading to a configuration where the perturbed vortex lines of both layers are 180° out-of-phase. However, as before, the amplification of the wavy dislocation of the vortex lines in the upper layer is larger than in the lower one. Thus, the streamwise vortices formed in the upper layer are now stronger than those in the lower layer. This effect also results in the orientation of the streamwise vortices closer to the flow x-direction and thus, the loss of their λ shape.

When both perturbations (horizontal and vertical) were introduced 180° out-of-phase (the peaks of the corrugations 180° out-of-phase with the tips of the indentations), our flow visualization revealed that depending on the relative

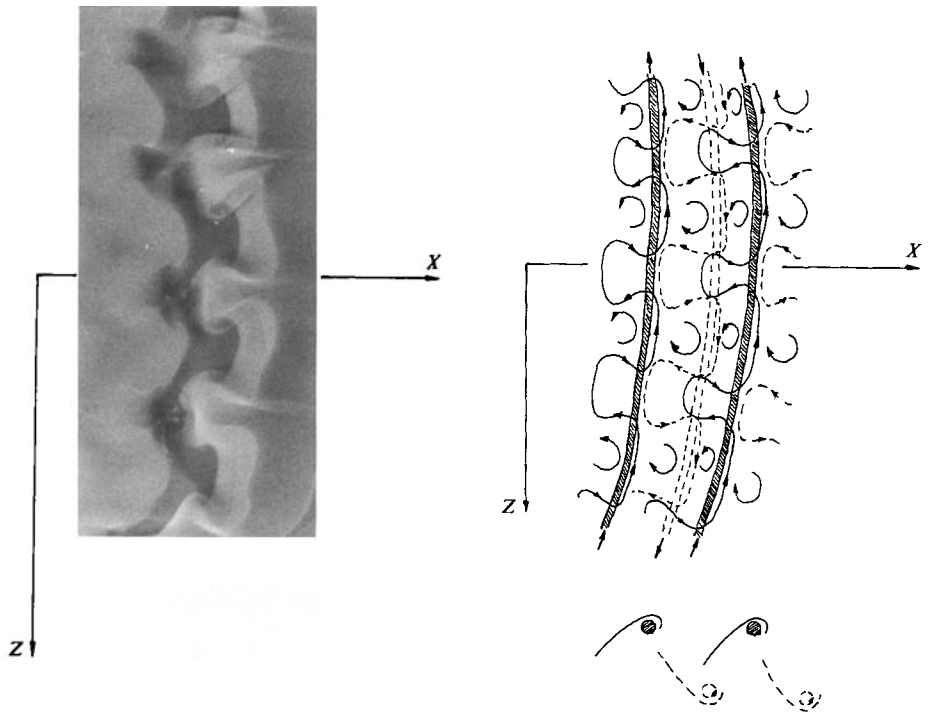

FIGURE 25. Effect of the horizontal perturbation. Plan view of the interface separating the two sides of the wake. A sketch of the corresponding vorticity configuration showing the array of alignment vortex loops is also given.

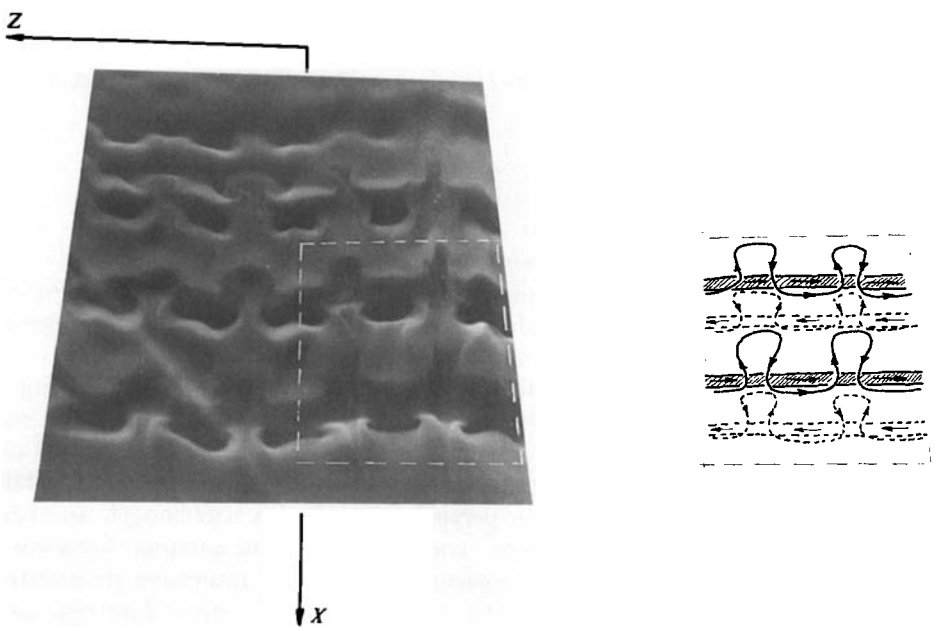

FIGURE 26. Effect of the horizontal perturbation. Perspective view of the interface separating the two sides of the wake.

amplitude of each perturbation, the flow develops either the three-dimensional configuration given in figure 19 or the one given in figure 24. Again, depending on the relative magnitude of the amplitude of both perturbations, the linear superposition of the two effects was found to cause either the amplification, suppression, or shifting of the two perturbations in the upper and lower layer. Because the 180° phase shift always results from the reorientation of the vertical perturbation, now the effect of the horizontal one (indentation) was always found magnified in the lower layer while it was decreased, cancelled or reversed in the upper one. Again, as was the case with the two perturbations in-phase, the only differences between the purely horizontally or vertical perturbation cases and these 180° out-of-phase combined ones, are that now the strength of the streamwise vortices are different in the two consecutive planes of positive strain (braids) and that the evolving streamwise vortices keep a flow (x) orientation rather than a λ shape.

6.3. *Effect of the wavelength of the periodic spanwise perturbation*

We have demonstrated that the plane wake under the effect of a perturbation of a given wavelength having both vertical and horizontal components develops either a symmetric or non-symmetric three-dimensional vorticity field. Furthermore, which mode develops depends on the relative amplitude of the horizontal and vertical components of the perturbation.

The rate of amplification of the wavy dislocation of the vortex filaments in the braids is given by the magnitude of the positive strain field created by the Kármán vortices. Thus, for a given wavelength (λ) of the Kármán vortices, dislocations of the filaments may grow at different rates depending on their spanwise wavelength due to viscous effects. However, since we have limited our study to relatively long wavelengths of the perturbations and thus, to an almost inviscid evolution of the vorticity, the growth rate of each perturbation should be almost equal.

We have conducted experiments where the perturbation wavelength λ' was $\frac{1}{3}$, $\frac{2}{3}$, 1, $\frac{4}{3}$ and $\frac{5}{3}$ of the Kármán vortices wavelength λ. For all these cases, no appreciable difference in the growth rate was observed in either the horizontal- or vertical-perturbation cases.

7. Conclusion

We have presented a combined experimental and numerical investigation of the three-dimensional evolution of a plane wake behind a flat plate subjected to perturbations periodically placed along the span. The flow was experimentally studied through flow visualizations of the interface separating the two sides of the laminar wake emerging from two laminar boundary layers. In addition, we numerically simulated an equivalent, temporally growing wake flow using nearly inviscid three-dimensional vortex dynamics methods. Due to the limitations of the vortex-filament techniques used in this study, however, our analysis was restricted to only the cases where the spanwise perturbations had a wavelength an order of magnitude larger than the filament core radius. Comparisons between the experimentally visualized and the numerically calculated interfaces demonstrated that the simulated flowfield exhibited the same qualitative features as the experimental ones. We can thus conclude that even for relatively low Reynolds numbers (≈ 100), the early stages of the three-dimensional evolution of plane wakes are dominated by the redistribution, reorientation, and stretching of vorticity rather

than by viscous effects. Hence, these flows can be modelled on the basis of their vorticity dynamics.

Depending on the orientation of the initial perturbation, the three-dimensional vorticity field of the wake was found to develop either a symmetric or a non-symmetric configuration. (A comparative summary of the characteristics of these two vorticity modes is given in the interface flow visualizations presented in figures 27, 28 and 29.) Both topologies of the vorticity field, however, exhibited the presence of closed vortex loops.

From the combined experimental and numerical information obtained in the case of the plane wake evolving behind the splitter plate with a corrugated trailing edge, we were able to give a detailed qualitative description of the mechanism governing the early stages of its three-dimensional evolution. This mechanism consisted of the following sequences. First, we observed the tilting of the initially transverse vorticity component into the flow direction under the action of the global shear. The concentration of spanwise vorticity in the Kármán vortices subsequently led to the formation of free stagnation points. These were not located at the centre of the braids (in contrast to the case of the single shear layer) but closer to the downstream roller. As a result, we saw the emergence of strong streamwise vorticity only in the downstream half of the braids. The interaction of the streamwise vorticity of both layers along with the continuous rotation of the principal planes of positive strain caused the streamwise vorticity to evolve into λ-shaped structures, similar to the ones known to exist in plane boundary layers. These horseshoe-like structures were seen to be in anti-phase on the two sides of the wake, thus breaking its initial symmetry. As they started to wrap around the Kármán vortices of the opposite layer, a staggered array of closed vortex loops were observed emerging in the global vorticity field.

For the case of the flow emerging behind a splitter plate with an indented trailing edge, we found a fundamentally different topology of the vorticity field. In this second case, the perturbed vortex lines of both layers were oriented initially and throughout the stretching always in the direction of the evolving planes of positive strain. Consequently, the streamwise vortical structures of both sides of the wake were found to remain in phase with each other throughout the stretching process. As the stretching reached large amplitudes, the global vorticity field exhibited closed vortex loops aligned in the flow direction, preserving the symmetry of the wake. Such a structure of closed vortex loops aligned in the streamwise direction was also observed by Breidenthal (1980) in the flow behind a flat plate with strong indentations in its trailing edge for cases with much higher Reynolds numbers. Thus, we infer that the described mechanism, although obtained from an investigation of a laminar wake formed by two laminar streams might also govern the evolution of the large-scale features in plane turbulent wake flows at high Reynolds numbers.

A brief study of the flows evolving from the combined horizontal and vertical trailing edge showed that depending on the relative magnitude of each perturbation component (horizontal and vertical) the wake developed either the symmetric or the non-symmetric three-dimensional vorticity configuration described above. Thus, the vorticity field (to a first approximation) can be described as a linear superposition of the two effects.

For the relatively long wavelengths of spanwise perturbations investigated in this study ($\lambda' \approx \lambda$), we did not observe a range of maximum amplification. This suggests that a whole bandwidth of spanwise wavelengths grow at comparable rates as can be inferred from the assumption of near inviscid dynamics. Since no preferred

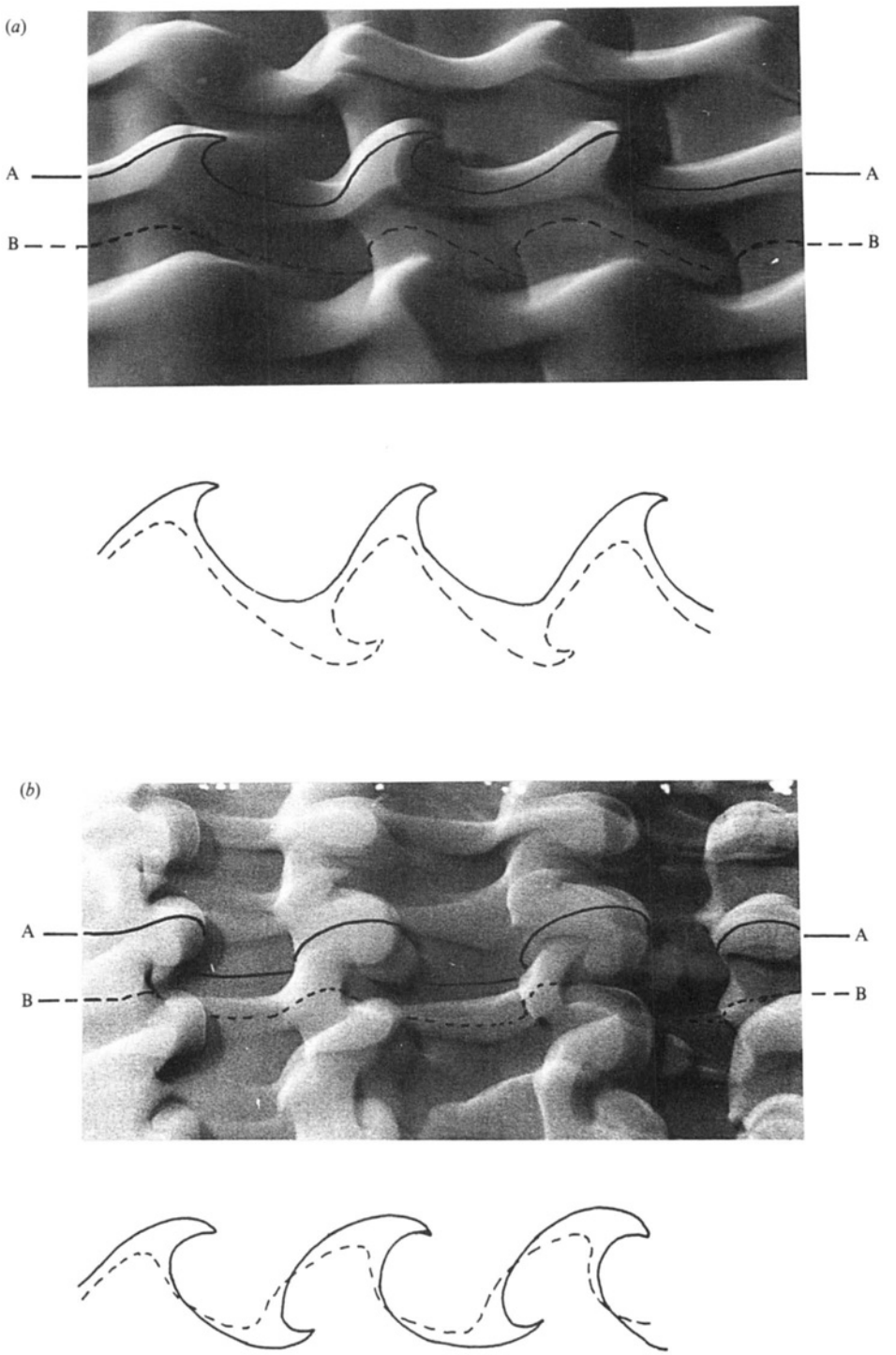

FIGURE 27. Comparative interface visualization of the two vorticity modes (near-side views). (*a*) Non-symmetric one resulting from the vertical perturbation. Corrugated splitter plate. (*b*) Symmetric one resulting from the horizontal perturbation. Indented splitter plate. The cross-sections A–A and B–B are in the two cases a half wavelength apart.

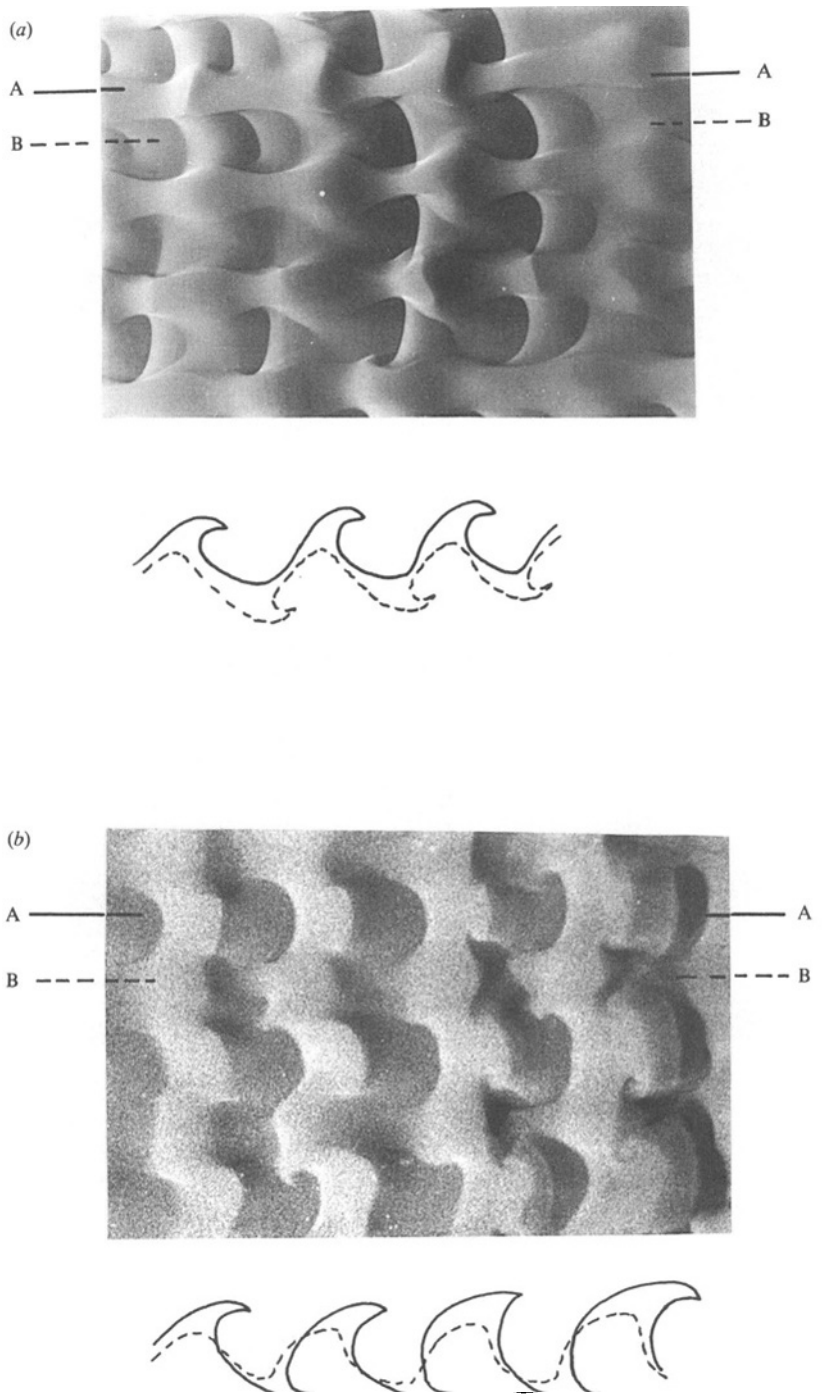

FIGURE 28. Comparative interface visualization of the two, vorticity modes (plan views of the interface). (*a*) Corrugated splitter plate. (*b*) Indented splitter plate. Sections ——, A–A are a half wavelength from – – – –, B–B.

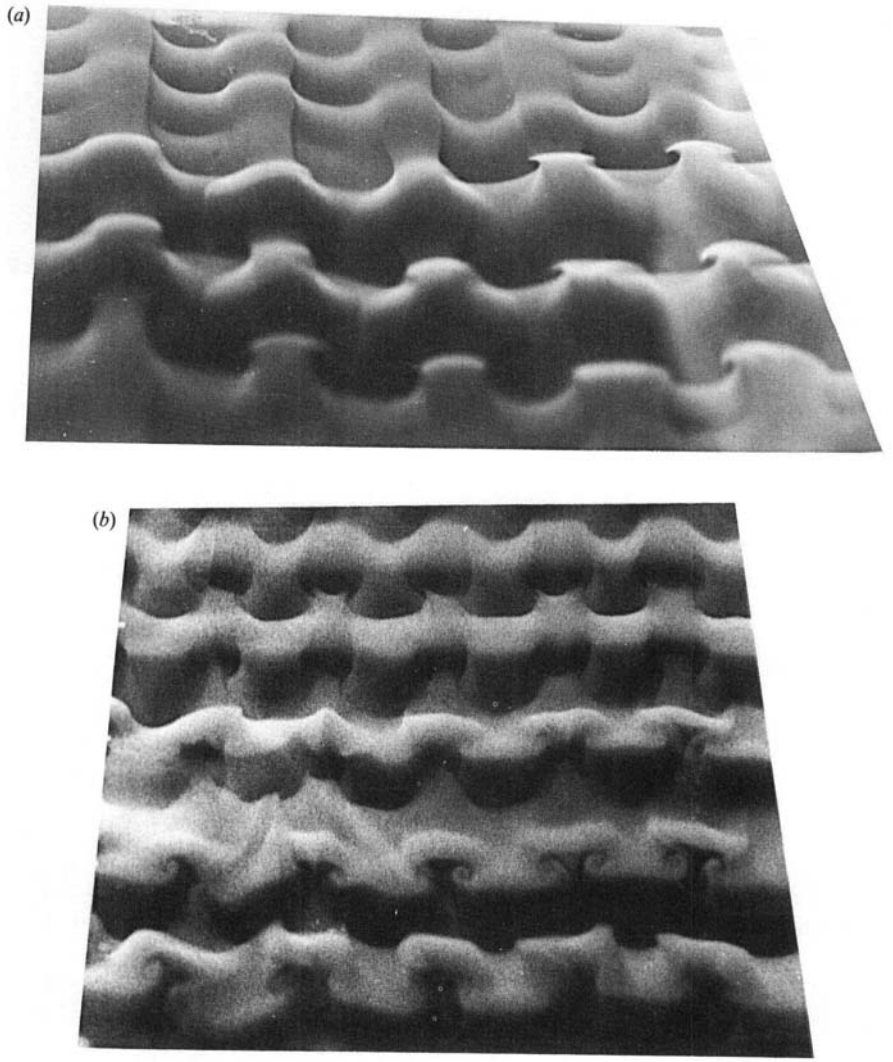

FIGURE 29. Comparative interface visualization of the two vorticity modes (near-end views).

wavelength was detected, the introduction of small upstream perturbations of a certain wavelength might significantly affect the spanwise wavelength of the fully developed three-dimensional flow.

The authors gratefully acknowledge discussions held with Professor Tony Maxworthy and Dr W. T. Ashurst on the physical and numerical aspects of the problem. Their reviews and comments on the original manuscript are greatly appreciated. Special thanks are extended to Mr H. Choi for his assistance during the acquisition of the photographic data. The test rig used in this study is a modified version of the one designed by Winant & Browand (1974). We would like to thank Professor Frederick K. Browand who generously made his water channel available to us. This work was partially supported by a grant from the US–Spain Joint Committee for Scientific Cooperation (Project number CCA-8510-057) and by a grant from San Diego Supercomputing Center. E.M. was at DFVLR, Göttingen, West Germany while most of the numerical simulation was done.

REFERENCES

AREF, H. & SIGGIA, E. D. 1981 Evolution and breakdown of a vortex street in two dimensions. *J. Fluid Mech.* **109**, 435.

ASHURST, W. T. & MEIBURG, E. 1988 Three-dimensional shear layers via vortex dynamics. *J. Fluid Mech.* **189**, 87.

BATCHELOR, G. K. 1967 *An Introduction to Fluid Dynamics.* Cambridge University Press.

BERGER, E. & WILLE, R. 1972 Periodic flow phenomena. *Ann. Rev. Fluid Mech.* **4**, 313.

BREIDENTHAL, R. 1980 Response of plane shear layers and wakes to strong three-dimensional disturbances. *Phys. Fluids* **23**, 1929.

CIMBALA, R. 1985 Large structure in the far wakes of two-dimensional bluff bodies. Ph.D. thesis. California Institute of Technology, Pasadena, CA, USA.

CORCOS, G. M. & LIN, S. J. 1984 The mixing layer: deterministic models of turbulent flow. Part 2. The origin of the three-dimensional motion. *J. Fluid Mech.* **139**, 67.

GRANT, M. L. 1958 The large eddies of turbulent motion. *J. Fluid Mech.* **4**, 149.

KOCH, W. 1985 Local instability characteristics and frequency determination of self-excited wake flows. *J. Sound Vib.* **99**, 53.

LASHERAS, J. C., CHO, J. S. & MAXWORTHY, T. 1986 On the origin and evolution of streamwise vortical structures in a plane, free shear layer. *J. Fluid Mech.* **172**, 231.

LASHERAS, J. C. & CHOI, H. 1988 Three-dimensional instability of a plane free shear layer. An experimental study of the formation and evolution of streamwise vortices. *J. Fluid Mech.* **189**, 53.

LEONARD, A. 1980 Vortex methods for flows simulation. *J. Comp. Phys.* **37**, 289.

LEONARD, A. 1985 Computing three-dimensional incompressible flows with vortex elements. *Ann. Rev. Fluid Mech.* **17**, 523.

LIN, S. J. & CORCOS, G. M. 1984 The mixing layer: deterministic models of a turbulent flow. Part 3. The effect of plane strain on the dynamic of streamwise vortices. *J. Fluid Mech.* **141**, 139.

MEIBURG, E. 1986 Numerical simulation of the formation of two- and three-dimensional structures in shear layers and wakes. Ph.D. thesis. Universitat Karlsruhe, West Germany.

MEIBURG, E. 1987 On the role of subharmonic perturbations in the far wake. *J. Fluid Mech.* **177**, 83.

MEIBURG, E. & LASHERAS, J. C. 1987 Comparison between experiments and numerical simulations of three-dimensional plane wakes. *Phys. Fluids* **30**, 623.

MORKOVIN, M. V. 1964 Flow around circular cylinder – kaleidoscope of challenging fluid phenomena. *Proc. ASME Symp. on fully separated flow.*

MUMFORD, J. C. 1983 The structure of the large eddies in fully turbulent shear flows. Part 2. The plane wake. *J. Fluid Mech.* **137**, 447.

PAYNE, F. & LUMLEY, J. 1967 Large eddy structure of the turbulent wake behind a circular cylinder. *Phys. Fluids Supp.* S194–S196.

ROGERS, M. M., MOIN, P. & REYNOLDS, W. C. 1986 The structure and modeling of the hydrodynamic and passive scalar fields in homogeneous turbulent shear flows. *Rep. no. TF* 25, Thermoscience Division, Department of Mechanical Engineering. Stanford University.

ROSHKO, A. 1954 On the development of turbulent wakes from vortex streets. *NACA Rep.* 1191.

ROSHKO, A. 1976 Structure of turbulent shear flows: a new look. *AIAA J.* **14** 1349.

TANEDA, S. 1977 Visual study of unsteady separated flows around bodies. *Prog. Aerospace Sci.* **17**, 287.

TOWNSEND, A. A. 1979 Flow patterns of large eddies in a wake and in a boundary layer. *J. Fluid Mech.* **95**, 515.

WINANT, C. D. & BROWAND, F. K. 1974 Vortex pairing: the dynamics of turbulent mixing layer growth at moderate Reynolds number. *J. Fluid Mech.* **63**, 237.